Environmental Challenges
Article In Press
Acceptation date : May 2025
https://doi.org/10.1016/j.envc.2025.101177
https://archimer.ifremer.fr/doc/00952/106420/

Assessing Geological and Seismic Hazards of Malili-Matano Region, East Luwu Regency, Sulawesi: A Preliminary Study for CCS and Strategic Infrastructure Planning

Soehaimi Asdani [1], Padmawidjaja Tatang [2], Subagio Subagio [2], Mandi Ibrahim [3], Tohari Adrin [1], Suharsono Suharsono [1], Menier David [4], Mathew Manoj [5], Ramkumar Mu [6], Novico Franto [1, 7, *]

[1] Research Center for Geological Disaster, National Research and Innovation Agency, Bandung, West Java, Indonesia
[2] Research Center for Geological Resources, National Research and Innovation Agency, Bandung, West Java, Indonesia
[3] Research Center for Geological Survey, Ministry of Energy and Mineral Resources, Bandung, West Java, Indonesia
[4] Geo Ocean, Univ Bretagne Sud, Univ Brest,CNRS, Ifremer, UMR6538, F-56000 Vannes, France
[5] Department of Geography, Geology and the Environment, Kingston University, Kingston-upon-Thames, Kingston, United Kingdom
[6] Department of Geology, Periyar University, Salem, India
[7] Marine Geological Institute, Ministry of Energy and Mineral Resources, Bandung, West Java, Indonesia

* Corresponding author : Franto Novico, email address : fran011@brin.go.id

Abstract :

Understanding the seismotectonic characteristics and seismic hazards of the Malili-Matano Region (MMR) in Sulawesi is crucial due to its proximity to active faults, including the Matano Fault Zone (MFZ) and surrounding fault systems. These geological conditions pose significant risks to infrastructure development, particularly Carbon Capture and Storage (CCS) facilities, which require a thorough assessment of seismic hazards. This study integrates seismotectonic mapping and Probabilistic Seismic Hazard Analysis (PSHA) to evaluate earthquake risks, with a particular focus on spectral acceleration (PSA) values that influence structural resilience.

The results indicate that MMR exhibits complex fault interactions, leading to elevated Peak Ground Acceleration (PGA) and Spectral Acceleration (PSA) values, with PSA Ss = 1.10 g at 0.2 seconds and S1 = 0.55 g at 1 second for Site Class SB under a 2% probability of exceedance in 50 years (2500-year return period). These seismic hazard estimates suggest that structural design in the region must adhere to Seismic Design Category D standards, including reinforced foundations and real-time ground motion monitoring to enhance CCS infrastructure safety. The study underscores the importance of continuous seismic monitoring, hazard mitigation strategies, and risk communication for infrastructure resilience in seismically active environments. The findings contribute to a refined understanding of seismotectonic behavior in MMR and its implications for CCS site selection and long-term sustainability.

Keywords : CCS, MMR, PSHA, seismotectonic, Sulawesi.

1. Introduction

CCS is crucial in mitigating greenhouse gas emissions, aligning with Indonesia's commitments to reduce its carbon footprint. However, the feasibility of CCS implementation faces significant challenges, particularly in site selection and cost estimations (Aromada et al., 2021). The dynamic nature of CCS technology, still in its developmental stages, contributes to variability in cost projections and the need for rigorous geological assessment.

The policy of a CCS development necessitates comprehensive evaluation and analysis, especially in seismically active regions. Indonesia's seismic landscape, exemplified by Malili-Matano region (MMR) within the Matano Fault Zone (MFZ), highlights the need for meticulous scrutiny. The intermittent occurrence of severe earthquakes in this region, documented by BMKG (2019), underscores the necessity of detailed seismic hazard assessments.

Although Malili does not currently host an active CCS project, it has been identified as a potential future CCS site due to its ultramafic rock formations and planned industrial expansion. The Pusat Survey Geologi, Geological Agency of Indonesia has conducted mapping and geophysical studies in Malili and Soroako to assess their potential for CO_2 storage and mineral trapping (PSG, 2022a, PSG, 2022b).

Additionally, Malili has been designated as a strategic industrial development area under the East Luwu Regency Long-Term Development Plan (PERDA Kabupaten Luwu Timur, 2005), with large-scale nickel smelting and metal refining operations currently in planning. The Indonesian government has outlined criteria for Injection Target Zones (ZTI) in MEMR No. 2/2023, and while Malili is not yet classified as an official ZTI, its geological and industrial characteristics suggest it may be considered for CCS feasibility assessments in the future (MEMR No. 2/2023). However, the intermittent occurrence of severe earthquakes in this region, documented by BMKG (2019), underscores the necessity of detailed seismic hazard assessments.

Seismotectonic maps and seismic hazard analysis are essential, providing important insights into infrastructure development plans on seismic stability. The seismotectonic analysis examines the relationship between geological structures and seismic activity, identifying fault lines, stress fields, and historical seismic events that could impact CCS site integrity (e.g., Cheng et al., 2023; Pettersson et al., 2022; Bredesen, 2022; Kim et al., 2020; Jing et al., 2019). Seismicity hazard analysis assesses the probability and potential impact of earthquakes, employing techniques like PSHA to quantify risks and inform infrastructure design (e.g., Rudman et al., 2024; Moratto et al., 2023; Ansari et al., 2022; Sianko et al., 2020; Chiou and Youngs, 2014).

Research in seismotectonic analysis e.g., Nazarinezhad et al., 2024; Escuder-Viruete et al., (2024) on the seismotectonic framework highlights the complex interplay of tectonic plates contributing to seismic hazards. Similarly, Sycheva (2024) emphasized integrating geological and geophysical data to enhance seismic hazard assessment accuracy. The research aims develop a seismotectonic map and assess seismic hazards through PSHA in MMR, ensuring that seismic risks are fully considered in future CCS feasibility assessments, PSG (2022a) and PSG (2022b). The findings will contribute to the safe implementation of CCS infrastructure in MMR**,** aligning with Indonesia's long-term carbon reduction commitments and seismic safety regulations

1.2. Geology Setting

Sulawesi Island, located along an active plate boundary, exhibits a complex geological landscape with diverging arms in the north, south, east, and southeast (Katili, 1991). As elucidated by Simanjuntak & Barber, 1996, and supported by Nugraha et al. (2022). The collision between the microcontinental blocks, specifically the Tukang Besi and Banggai-Sula blocks, and the eastern part of Sulawesi is estimated to have begun in the Early Miocene, approximately 20 million years ago, and continued into the Middle Miocene. This tectonic event catalyzed a series of regional phenomena, including the obduction of ophiolites in East Sulawesi, leading to the formation of a thrust fault belt and the development of the Palu-Koro left-lateral fault as a transcurrent fault.

Sulawesi's tectonic framework entails the Pluto-Volcanic Arcs in the western and northern regions of Sulawesi, characterized by volcanic activity and tectonic activity associated with subduction zones, **Fig. 1**. The Central Sulawesi Metamorphic Belt encompasses metamorphic rocks formed through intense heat and pressure, indicative of significant geological processes. The East Sulawesi Ophiolite Belt is marked by the presence of ophiolite complexes, signifying the obduction of oceanic crust onto continental crust. Lastly, the Microcontinent Fragments of Banggai-Sula and the Tukang Besi Archipelago constitute remnants of ancient continental fragments, providing insights into the region's geological history.

In the context of MMR, the MFZ plays a crucial role in understanding the local geohazards and seismic risks associated with CCS implementation. The MFZ, located between the Central Sulawesi Metamorphic Belt and the East Sulawesi Ophiolite Belt, is characterized as a left-lateral strike-slip fault mechanism (Patria et al., 2023). This fault extends through various geological formations and is an active fault zone in Central Sulawesi. Stress accumulation along this fault zone poses significant risks to the impermeable cap rock essential for CCS operations. Fault reactivation could compromise cap rock integrity, leading to potential leakage. These risks emphasize the importance of incorporating fault displacement and seismic loading considerations into CCS infrastructure design. The active nature of this fault zone and its interaction with surrounding geological formations are critical considerations for seismic hazard assessments and site selection for CCS projects.

2. Material And Methods

2.1. Geology and Geophysics Investigations

Geological and geophysical investigations (**Fig. 2**) were conducted in 2022 to produce a higher-resolution geological map of the Malili Quadrangle compared to the map by Simanjuntak et al. (2007). Our field survey enhanced resolution through advanced measurement techniques and additional data acquisition. Four observation locations were strategically selected based on criteria such as representation of key lithological units, clear exposure of fault structures, potential relevance to upper structure analysis, and ease of access during fieldwork. Due to limitations in vertical stratigraphic data, we were unable to document detailed transect lines and stratigraphic sections at each observation location as comprehensively as in Nugraha et al. (2023). In addition, our seismotectonic map significantly improves upon previous work by identifying six distinct fault zones rather than the two zones reported by Simanjuntak et al. (2007) by integrating additional data such as regional seismicity and focal mechanism analyses. These enhancements provide a more robust framework for evaluating the geological and seismotectonic conditions of the area, which is critical for assessing its potential for upper structures CCS and strategic infrastructure planning.

The field survey identified dominant lithologies, including metamorphic rocks from the Central Sulawesi Metamorphic Belt and ophiolitic sequences. Outcrop observations revealed deformed metasediments, fault gouges, and evidence of shearing along major structural trends. Additionally, the presence of highly fractured schists and quartzites suggests regional metamorphism, while exposures of serpentinized peridotite and ultramafic rocks confirm the continuity of the East Sulawesi Ophiolite Complex in this region. Karst formations and sedimentary deposits along fault-controlled valleys were also documented, providing further insights into subsurface geological structures and their relation to seismic hazards.

To complement surface geological observations, gravity anomaly data were also obtained using Lacoste and Romberg instruments. The gravity measurement site was selected to minimize near-surface noise and provide a regional-scale perspective on subsurface density variations, ensuring a more comprehensive Bouguer Anomaly Map. This approach enhances the resolution of regional mapping beyond previous studies (Mirnanda and Siagian, 2007) and allows for the identification of deeper fault structures. The most recent data on gravity anomalies were used to detect and analyze anomaly patterns at both regional and local levels using low-pass and high-pass filtering techniques, improving the interpretation of the tectonic framework in the MMR.

To analyze subsurface structures, low-pass and high-pass filtering techniques were applied to separate regional and local anomalies. A low-pass filter with a cutoff wavelength of 50 km was used to emphasize deep-seated regional anomalies, while a high-pass filter with a cutoff wavelength of 5 km was applied to enhance shallow subsurface structures. These filtering parameters were selected based on studies in similar tectonic environments (Zakariah et al., 2021) and validated by comparing filtered outputs with established geological structures.

Spectral analysis was used to estimate the depth of gravity anomaly sources, thereby distinguishing between shallow and deep-seated fault structures (Zakariah et al., 2021). This approach separates anomalies based on their frequency content in the gravity field. Further refinement of fault segmentation was achieved using second vertical derivative (SVD) analysis, which effectively enhances short-wavelength features and aids in delineating fault structures (Blakely, 1996; Pirttijärvi, 2004; Permatasari et al., 2019; Ali et al., 2023).

Although low-pass filtering can reveal regional-scale anomalies indicative of deep-seated fault structures, we did not generate a dedicated deep fault map in this study due to the absence of direct validation data (e.g., borehole or well-log information) essential for confirming deep fault interpretations. Relying solely on gravity anomaly filtering to infer deep faults carries inherent uncertainties; therefore, our primary focus remains on seismotectonic mapping and seismic hazard assessment based on surface geological structures, seismicity data, and gravity anomalies to delineate near-surface fault systems.

While Euler deconvolution is a widely used technique for estimating fault depths, we opted not to include it in this study because it requires assumptions about the structural index that could introduce additional uncertainties without supporting borehole data. Nonetheless, we acknowledge that Euler deconvolution can provide valuable insights into subsurface fault geometry and will be considered in future research.

Hence, the integration of geological, geophysical, and seismicity data provides a comprehensive framework for interpreting the geological characteristics of faults within MMR, including LM. This study incorporates multiple geophysical techniques, including high-pass and low-pass filtering, spectral analysis for depth estimation, and second vertical derivative (SVD) to enhance fault delineation. The resulting parameters contribute to the development of a seismotectonic map, a widely used approach in various tectonic settings, such as in Iran (Nazarinezhad et al., 2024), Hispaniola (Escuder-Viruete et al., 2024), and Turkey (Sycheva, 2024). Subsurface structures were derived by interpreting local anomaly patterns, employing second vertical derivative (SVD) analysis to delineate existing fault structures as shown by other studies (e.g., Blakely, 1996; Pirttijärvi, 2004; Permatasari et al., 2019; Ali et al., 2023).

Therefore, the geological-geophysical and seismicity data can be used to interpret the geological characteristics of faults within MMR, including LM. Those parameters will produce a seismotectonic map, a common approach that has been applied in many places, such as in Iran by Nazarinezhad et al. (2024), Hispaniola by Escuder-Viruete et al. (2024) and by Sycheva (2024) in Turkey.

2.2. Earthquake Catalog

Earthquake catalog data were compiled from three primary sources: the Global Centroid Moment Tensor Project (GCMT, 2022), the United States Geological Survey (USGSEC, 2022), and the International Seismological Centre (ISC, 2020). Data from 1907 to 2022 included a range of magnitudes ($4.4 \leq MW \leq 8.1$) and depths (1 to 640 km), resulting in a total of 5,313 records after filtering duplicates, **Fig. 1**. The depth range affects PSHA by distinguishing between shallow events, which often result in higher ground shaking intensity, and deeper events, which may contribute to broader regional hazards due to their larger rupture areas. A linear regression model was utilized to standardize diverse magnitude types to a uniform scale (Mw), addressing non-homogeneous distributions across magnitude scales based on 687 events. Approximately 72% of the earthquakes in the catalog occurred at depths shallower than 40 km, classified as shallow earthquakes, which are known to produce more intense local shaking. The remaining 28% of the events occurred at depths exceeding 40 km, classified as intermediate-to-deep focus earthquakes, which tend to generate broader regional shaking effects. This depth distribution is a critical factor in PSHA modeling, as shallow earthquakes predominantly control localized ground motion, whereas deeper seismic events influence long-period wave propagation. This analysis involved determining the best-fit line to relate different magnitudes, following the approach of Scordilis (2006), and the resulting trend line equation for magnitude conversion is presented in **Fig. 3**.

2.3. Seismic Source Characterization and Zonation

Characterizing seismic sources involves identifying relevant regional earthquake sources, essential for probabilistic seismic hazard assessment (PSHA). The geological subdivision of faults into segments (**Table 1)** aids in understanding potential seismic sources, as illustrated in **Fig. 4**. The segmentation was based on multiple geological and geophysical parameters, including geomorphological features, seismicity patterns, variations in slip rates, and historical earthquake records. Fault traces were examined using remote sensing data and topographic relief to identify distinct segment boundaries, while earthquake epicenters were mapped along fault structures to detect clustering indicative of segment divisions. Additionally, differences in slip rates derived from geodetic and geological studies helped define fault segments with distinct deformation characteristics. Historical seismicity data further constrained the segmentation, ensuring that each fault zone exhibited unique rupture behavior.

This segmentation aligns with methodologies used in other tectonic regions (e.g., Wesnousky, 1988; Pettersen et al., 2014) to maintain consistency in fault modeling for PSHA. Moreover, this classification contributed to the delineation of six seismotectonic zones (I-VI) that represent variations in structural geology and seismic activity within the Malili-Matano region. Unlike the previous classification by Simanjuntak et al. (2007), which identified only two major fault strands, our analysis reveals a more detailed segmentation, reflecting the complex interactions between fault systems and regional tectonic stress fields. This refined seismotectonic zonation provides a basis for assessing site-specific seismic hazards and engineering considerations for potential infrastructure developments, including CCS feasibility. The annual seismicity rate was estimated for each zone using the Gutenberg and Richter (1944) recurrence law, establishing a model for seismic activity in the area. Constants a and b derived from statistical analysis of historical observations were crucial in characterizing earthquake distributions across different zonations, **Fig. 5**.

2.4. Ground Motion Prediction and Site Classification

Ground Motion Prediction Equations (GMPEs) estimate ground shaking intensity based on earthquake magnitude, distance from the source, and local soil conditions. This study utilized the Chiou and Youngs (2014) model, chosen for its applicability to tectonically active regions similar to the study area. Key inputs included moment magnitude, distance metrics, and shear wave velocity. Site classifications identified rock sites with average shear wave velocities between 750 to 1500 m/s, corresponding to Rock Classification SB (SNI, 2019). While this classification primarily informs ground motion estimates for seismic hazard analysis, it is particularly relevant for upper structures such as CO_2 injection facilities and monitoring stations. Although CCS targets deep geological formations for CO_2 storage at depths exceeding 2500 m, as observed in the Donggi-Matindok PSC (Djiada, 2024), understanding surface seismic hazards remains crucial for site selection and infrastructure resilience (Rasool et al., 2023).

2.5. Probabilistic Seismic Hazards Assessment

The PSHA was conducted using a total probability approach (e.g., Jorjiashvili et al., 2018; Liu and Chang, 2015), integrating seismic source models based on fault lines and historical seismicity. The OpenQuake software (e.g., Pagani et al., 2014; GEM, 2018) was employed for computational assessments using empirical GMPE models, reflecting regional seismic characteristics (Chiou and Youngs, 2014). Two probabilistic levels were analyzed: 2% probability in 50 years relevant to general infrastructure planning, and 7% probability in 75 years typically used for critical infrastructure standards, such as bridges (SNI, 2016). While these standards are not explicitly designed for CCS facilities, they provide a useful reference for evaluating seismic hazards in surface structures. Future CCS site assessments should align with MEMR No. 2/2023, which outlines geological requirements for CO_2 storage sites. However, a comprehensive seismic hazard framework specifically for CCS surface infrastructure in Indonesia is yet to be developed.

3. Results and discussion

3.1. Geology of MMR

The MFZ, which lies from northwest to southeast Sulawesi (**Fig. 1**), is located between the Central Sulawesi Metamorphic Belt and the East Sulawesi Ophiolite Belt. The Central Sulawesi Metamorphic Belt is limited to the middle and part of the Southeastern Arm of Sulawesi, which is assumed to result from a collision between the Gondwana Fragment and the active margin of Asia in the Late Oligocene or Early Miocene, Villeneuve et al. (2002). This area comprises sheared metamorphic rocks, including the Pompangeo Skis Complex and the Melange Complex (e.g., Parkinson, 1998a; Parkinson, 1998b; Parkinson et al., 1998), including Miocene ophiolites as the Lamasi Complex, Bergman (1998). This area is assumed to be the Accretions Complex formed in the Cretaceous and Paleogene, Katili (1991) as a suture between Sulawesi's western and eastern parts, Villeneuve et al. (2002). The main structure consists of a fold belt and thrust fault. The thrust fault structure faces up to the Makassar Strait at north-south trending (Villeneuve et al., 2002; Coffield et al., 1993), and a left lateral fault system in Central Sulawesi, consisting of the Palu-Koro Fault and the Matano Fault based on radiometric dating estimates that fold belts developed from 13-5 million years ago, (e.g., Bellier et al., 2006, Watkinson and Hall, 2017, Patria et al., 2023).

The East Sulawesi Ophiolite Belt extends from Central Sulawesi and continues across the East and Southeast Arms, including the Muna and Buton Islands. It consists of tectonically dismembered and highly fractured ophiolite associated with Mesozoic metamorphic rocks and sediments (e.g., Simanjuntak and Barber, 1996; Kadarusman et al., 2004), **Fig. 2**. This ophiolite series comprises residual mantel peridotite, mafic-ultramafic cumulate and gabbro, sheeted dolerites, and basalt volcanic rock. The oceanic plateau component of ophiolite has been interpreted as a product of the Southeast Pacific Superplume, Kadarusman et al. (2004).

Referring to the site investigation and regional geological map by Simanjuntak et al. (2007), tectonic stratigraphy has been carried out in and around the MFZ to the LM area. The result shows that this zone consists of the Pre-Oligo-Miocene tectonic period, the Pre-Plio-Pleistocene tectonic period, and the Post-Plio-Pleistocene tectonic period (Quarternary). The tectonic period of the Pre-Oligo-Miocene has deformed the Ultrabasic Complex/MTosu, Wasuponda Melange/MTmw, and Matano Formation/Kml. The Ultrabasic Complex/MTosu as the oldest formation consist of hatzburgite, lherzolite, wehrlite, websterite, serpentinite, dunite, gabbro and diabas. The outcrop of MTosu can be found in **Figs. 2A, 2B, and 2C.** Wasuponda Melange/MTmw consists of an exotic block of serpentinite, schist amphibolite, meta dolerite, foliated limestone, ultramafic rock, eclogite, and red scaly clay. The Matano Formation/Kml consists of crystallin limestone, calcilutite, marl, and shale, as present in **Fig. 2D**. The unconformity above three old formations found in the Larona Formation (Tpls) consists of sandstone, conglomerate, claystone, and tuff, and the Tomata Formation (Tmpt) consists of shale, sandstone, marl conglomerate, and lignite as can be seen in **Fig. 2D**. Both formations belong to Middle Miocene to Late Miocene age. The region's youngest formations are the LM deposit and coastal and river alluviums.

The geotectonic of the MFZ is a part of the transition tectonic between the tectonics of the Central Sulawesi Metamorphic Belt and East Sulawesi Ophiolite Belt. The boundary of these two tectonic belts is characterized by the MFZ, which shows the character of the left lateral strike-slip fault mechanism. This fault extends through the Ultrabasic Complex, Wasuponda Melange, the more recent Tomata and Larona formations (middle-late Miocene), and other newer strata of LM deposits. Therefore, it can be stated that the Matano active fault zone is an active fault zone in Central Sulawesi. Based on the tectonic setting and geological structure developed in this area, it can be estimated that the main tectonic forces of this region are generated in the southwest-northeast direction. The tectonic forces that have worked so far have resulted in the left lateral Matano Active Fault Zone. The northern fault block moves relatively to the west from the southern fault block, while the south fault block moves relatively to the east from the north fault block. As a result of the activity of this active fault, the tension and shearing active zones can be found along this fault zone, and this area is highly fractured.

3.2. Gravity Anomaly

Gravity measurements south of LM (**Fig. 2E**) delineate three regions: high, medium, and low residual anomalies. High residual anomalies range from 14 to 35.6 mGal, predominantly located southwest of LM. The medium residual anomalies range from -10 to 14 mGal in the southeast, south, and north of LM. Low residual anomalies range from -20 mGal to -10 mGal, as shown in **Fig. 6A**. The SVD anomaly gravity map (**Fig. 6B**) indicates values ranging from a minimum of 48.31 × 10^-8 mGal/m² to a maximum of 31.41 × 10^-8 mGal/m². The southern part of LM displays varied residual anomalies extending towards Bone Bay (BB), potentially associated with the surface patterns of the shallow structure.

3.3. Seismotectonic Map

Our seismotectonic analysis elucidates the geotectonic activity and the interplay between tectonics and seismic occurrences in the MMR. The multidisciplinary approach encompassed the assessment and interpretation of primary and secondary geological and geophysical data, including geomorphology, stratigraphy, lithology, structural geology, neotectonics, gravity, and seismicity. In addition to field observations of active fault traces and deformation structures. This led to the creation of a refined seismotectonic map of the MFZ (**Fig. 7**).

Unlike the previous classification by Simanjuntak et al. (2007), which categorized the MFZ into two primary fault strands, our study identifies six distinct seismotectonic zones based on geological evidence, morphological variations, and earthquake distribution patterns. The MFZ extends in a northwest-southeast direction, with a major fault trace cutting through the Matano Lake region. The segmentation of the MFZ was determined by identifying three seismotectonic zones north of the fault (Zones I, II, III) and three zones south of the fault (Zones IV, V, VI), each exhibiting unique lithological, structural, and seismological characteristics.

The northern section (Zones I-III) is characterized by significant fault branching and secondary thrust structures, as evidenced by outcrop observations of fault gouges, shear-related deformations, and displaced metasedimentary units. This section exhibits a dominant strike-slip mechanism with localized thrusting, indicating stress partitioning within the shear zone. Additionally, historical earthquake records show a concentration of moderate-magnitude seismic events in this region, reinforcing the active tectonic nature of these segments.

The southern section (Zones IV-VI), in contrast, is associated with ophiolitic and sedimentary deposits, with clear evidence of oblique-slip and normal faulting mechanisms. This suggests a more complex stress regime than previously recognized, with portions of the MFZ accommodating both horizontal and vertical displacements. The presence of multiple fault step-overs and segmented rupture planes further supports the classification of these areas as distinct seismic source zones.

This refined segmentation is supported by focal mechanism solutions and historical earthquake distribution patterns, which indicate variations in stress orientations and fault activity levels across different segments of the MFZ. The highest compressive stress is directed northeast, while the minimum compressive stress is oriented northwest-southeast (e.g., GCMT, 2022; Beaudoin et al., 2003; Patria et al., 2023). Additionally, differences in slip rates along the MFZ, as inferred from geodetic and geological studies, provide further validation for the presence of distinct fault segments with varying deformation characteristics.

The seismotectonic zoning framework adopted in this study is consistent with methodologies used in previous seismic source characterizations (e.g., Wesnousky, 1988; Pettersen et al., 2014). This refined fault segmentation model enhances the accuracy of PSHA by better representing potential seismic sources. Furthermore, the classification of these six zones provides critical insight into regional seismic hazard distribution and its implications for infrastructure planning, including CCS feasibility assessments in the MMR.

The occurrence of the 2017 Matano earthquake and the 2018 Palu-Koro earthquake further highlights the relevance of understanding fault segmentation and seismic source zones in the region. The 2017 event, located near LM, corresponds with activity along the central MFZ segments , supporting interpretations of active strike-slip deformation. In contrast, the 2018 Palu-Koro rupture, though outside the immediate study area, underscores the seismic potential of major fault systems in Sulawesi and their ability to trigger cascading hazards, including tsunamis and widespread infrastructure damage. These events emphasize the necessity of incorporating fault connectivity and segment interaction into regional hazard assessments, especially for strategic infrastructure planning in the Malili area.

3.4. PSHA Calculation

The PSHA utilizes various parameters to estimate seismic hazards. Key inputs are calculated manually, including the shear wave velocity at a depth of 30 meters (Vs30), which was set at 760 m/s based on geological and geotechnical considerations in the study area.

The Vs30 = 760 m/s value was selected because it represents the transition between NEHRP (2020) site class B (rock) and class C (very dense soil/soft rock), making it an appropriate choice for regions characterized by a combination of sedimentary deposits and basement rock formations (Boore et al., 1997; Allen and Wald, 2009). Given that the MFZ and its surrounding areas exhibit variable lithological conditions, Vs30 values in comparable tectonic settings generally range between 720–800 m/s. Studies in Sulawesi have also adopted similar Vs30 values for seismic hazard modeling, reinforcing the appropriateness of this choice (Irsyam et al., 2020).

Furthermore, the classification of seismotectonic zones (I-VI) played a crucial role in determining Vs30 values. Each seismotectonic zone represents a distinct geological setting, ranging from metamorphic and ultramafic basement rocks in the north to ophiolitic and sedimentary formations in the south. These variable geological conditions affect seismic wave propagation, justifying the use of Vs30 = 760 m/s as a representative site condition for the study area.

The depth to the top of rupture (ZTOR) and the hypocenter depth (ZHYP) remain crucial parameters in the PSHA analysis. If ZTOR is not specified, it is estimated from ZHYP, down-dip rupture width (W), and dip (δ), assuming the hypocenter is positioned 60% down the fault width, following the methodology of Mai et al. (2005). In cases where ZHYP is unknown, a linear relationship between ZHYP and magnitude (M) is used based on Scherbaum et al. (2004).

For strike-slip faults, characterized by rake angles within 30° of horizontal, ZHYP can be determined, allowing for the estimation of ZTOR using the method outlined by Mai et al. (2005). When the fault dip angle (δ) is unspecified, it is approximated using faulting style and rake angle guidelines from Kaklamanos et al. (2011), which revised earlier guidelines from Brian et al. (2006). The down-dip rupture width (W) is estimated based on earthquake magnitude and faulting style, utilizing logarithmic relationships presented by Wells and Coppersmith (1994). Additionally, the depth to the Vs = 1.0 km/s horizon (Z1.0) is a necessary input. When using the Chiou and Youngs (2014) models, Z1.0 can be estimated following Brian et al. (2014). The three distance measures (RJB, RRUP, and RX) and the three rupture parameters (ZTOR, δ, and W) are derived from geometric equations formulated by Kaklamanos et al. (2011). The calculation sequence begins with RX from RJB, α (source-to-site azimuth), W, ZTOR, and δ, followed by RRUP derived from RX and the relevant parameters.

3.4.1. PGA and 5% PSA

Fig. 4 highlights two significant seismic events within the study area. The first, labelled S2, recorded a peak magnitude of Mw 5.6 at a depth of 54.7 kilometers. The second event, S1, had a magnitude of Mw 4.7 at a shallower depth of 16.4 kilometers. Both events occur near multiple seismic sources, exhibiting distinct focal mechanisms: S2 primarily resulted from a strike-slip mechanism, while S1 stemmed from a left-lateral strike-slip fault mechanism. The PGA values recorded at these sites were 0.01 g for S1 and 0.039 g for S2. **Fig. 8** illustrates the 5% damped PSA values, providing insight into the ground motion characteristics during these events. Understanding these measurements is essential for evaluating potential impacts on structures and infrastructure, enabling comprehensive seismic hazard assessments.

Both the S1 and S2 locations lie within zones influenced by historical and recent seismicity, including the 2017 Matano and 2018 Palu-Koro earthquakes. These events demonstrate the variability in depth, rupture characteristics, and ground shaking intensities across the MFZ system. The Matano earthquake, occurring close to S1, illustrates the potential for shallow crustal fault activation in this area, which can lead to strong ground motions despite moderate magnitudes. The 2018 Palu-Koro event, while more distant, revealed the cascading effects of high-magnitude ruptures and underscored the interconnected nature of strike-slip fault systems across central Sulawesi. Understanding this analogy is essential for evaluating future seismic threats to critical infrastructure in the MMR.

PSHA for 2% Probability in 50 Years (2500-Year Return Period). The 2500-year return period (2% probability of exceedance in 50 years) was selected based on international seismic hazard assessment standards for high-risk infrastructure, including CCS facilities. This return period aligns with NEHRP (2020), ASCE (2010), and Petersen (2018)**,** which define safety margins for critical infrastructure subjected to extreme earthquake events.

Annual Probability Exceedance: For site S1, the computed PGA with a 2% probability of occurrence in 50 years is 0.371 g, with an annual probability exceedance of 0.00057. For site S2, the PGA is 0.465 g, corresponding to an annual probability exceedance of 0.00041. Additionally, for 75 years, site S1 has a 7% likelihood of experiencing a ground acceleration of 0.354 g, while site S2 shows a 7% probability of experiencing 0.445 g, **Fig. 10**. The annual probabilities for exceeding ground accelerations are 0.00051 for site S1 and 0.00045 for site S2.

PSHA Map: According to ASCE (2010), the site-specific MCER PGA is less than both the geometric mean of the 2,475-year return period PGA and the 84th percentile PGA. The PSHA Map for the MMR, where MFZ-LM is located, indicates a PGA range of 0.20 - 0.50 g. The spectral acceleration at short periods (PSA S_s) for 0.2 seconds (**Fig. 11**), ranges from 0.50 to 1.10 g, while the spectral acceleration at 1 second (PSA S_1) **Fig. 12**, ranges from 0.20 to 0.55 g, representing a 2% probability of occurrence within 50 years (2500-year return period). The PSA S_s values indicate the region's susceptibility to short-duration, high-frequency shaking, which is commonly associated with shallow crustal earthquakes. Conversely, PSA S_1 values reflect long-period ground motion, which is more influenced by deeper seismic sources and larger fault ruptures. This differentiation is critical for evaluating the potential vulnerability of different types of infrastructure, especially considering their natural resonance periods and structural flexibility. As mentioned in the PSHA map (**Fig. 10**), zones with lower seismic risk (PGA < 0.25 g) are characterized by sparse fault networks and lower stress concentrations. These regions, particularly in the southwestern part of MMR, are proposed as safer options for CCS infrastructure and strategic industrial development. The delineation provides critical guidance for minimizing seismic risks in infrastructure planning, complementing geological assessments, and future feasibility studies.

3.4.2. Hazard disaggregation

The disaggregation analysis was performed to determine the contributions of different magnitude and distance ranges to the total hazard at selected sites S1 and S2. The magnitude and distance ranges were determined based on historical seismicity data and expected rupture characteristics of the MFZ. To ensure statistical reliability, earthquake catalogs from ISC, and USGS were utilized, filtering events with Mw ≥ 4.0 to capture significant seismic activity. The distance ranges (10–50 km) were selected based on the maximum expected rupture length of active fault segments, following seismic hazard assessment methodologies in similar tectonic environments (e.g., Pettersen et al., 2014). The conditional probability of exceeding a given intensity measure (IM) is computed as:

$$P(M,R|IM) = \frac{P(IM|(M,R)P(M,R)}{\sum P(IM|M,R)P(M,R)}$$

where P(IM|M,R) is the probability of observing a given ground motion at a site given magnitude and distance, and P(M,R)is the probability of an earthquake occurring at a given magnitude and distance. Ground Motion Prediction Equations (GMPEs) were used to evaluate P(IM|M,R), while seismic source models provided probability distributions for P(M,R). This methodology follows Bazzurro & Cornell (1999) and McGuire (1995) and ensures a robust framework for PSHA.

Fig. 13 summarises the hazard disaggregation for the average return period of 2500 years for the two studied sites. The two horizontal axes represent the magnitude and distance ranges, while the vertical axis represents the relative contribution to the seismic hazard in terms of PGA exceedance probability (2% in 50 years).

The results indicate that S1, which is closer to the MFZ and LM, exhibits greater hazard contributions from smaller distance intervals than S2. Additionally, S2, although farther from the MFZ, is located on softer sedimentary deposits, which results in higher spectral acceleration values compared to S1, which is positioned on more stable basement rock formations (**Fig. 14**). These findings underscore the importance of incorporating local site effects and rupture characteristics into seismic hazard assessments.

3.4.3. Design Respons Spectra

Table 2 presents the MCE ground acceleration and response spectral acceleration for short-period spectral acceleration SS (0.2 seconds) and one-second spectral acceleration S1 at sites S1 and S2. These values were calculated using hazard disaggregation results, where the dominant magnitude-distance contributions to seismic hazard were determined based on historical earthquake data and expected rupture characteristics of the MFZ**.** The Amplification Factor for PSA is a coefficient that varies based on site class, with Fa and Fv values adopted from SNI (2019) for Class SB, consistent with ASCE (2010) and BSSC (1997) guidelines. Structures in this region are assigned Site Response Coefficients (Fa and Fv) following **Tables 3** and **Table 4** of SNI (2019). The adjusted MCE spectral response accelerations for short periods (SMS) and 1 second (SM1) are calculated following SNI (2019) guidelines. Design spectral response acceleration parameters SDS and SD1 are derived from the mapped values of SS and S1 according to the formulas provided by SNI (2019). The elastic design response spectrum for the site is depicted in **Fig. 14**, indicating that S2, situated near the MFZ and LM, exhibits higher values than S1. This difference is attributed to local site effects, geological conditions, and rupture directivity. S2 is underlain by softer sedimentary deposits, which amplify seismic waves, whereas S1 is located on harder basement rock, reducing amplification. Furthermore, S2 is positioned closer to the intersection of multiple fault segments, where complex wave propagation and directivity effects contribute to stronger ground motion. These findings are consistent with previous studies on on-site response and rupture directivity (e.g., Somerville et al., 1997).

3.4.4. Reflection on Previous Studies

Prior research conducted by Cipta et al. (2016), Irsyam et al. (2020), and Patria (2023) provided fundamental insights into the seismic risks in Sulawesi, particularly focusing on regional-scale assessments of seismic hazards. These studies identified the MFZ as a left-lateral strike-slip fault, yet fault segmentation and seismotectonic zoning within MMR were not explicitly defined. The PSHA model developed by Cipta et al. (2016) remained regional in scope, relying on broad ground motion prediction models that did not incorporate detailed fault segmentation, site-specific Vs30 values, or localized seismicity characteristics in MMR.

To address these limitations, this study introduces a more detailed seismotectonic model that integrates fault segmentation, seismicity data, and site response analysis. The application of hazard disaggregation techniques refines the PSHA, which was not performed in previous studies. Furthermore, by incorporating updated Vs30 values**,** this research provides a more accurate ground motion estimation for MMR, ensuring improved infrastructure planning and seismic risk mitigation strategies.

The regional seismic hazard model developed by Cipta et al. (2016) did not include a zonal analysis for MMR due to limited high-resolution seismic data and site-specific geological investigations. At the time, ground motion prediction models were based on broad regional datasets**,** without detailed fault segmentation or localized Vs30 values.

Our study improves upon these limitations by incorporating a refined seismotectonic framework that integrates geological, geophysical, and seismicity data specific to MMR. The updated PSHA includes hazard disaggregation techniques, enabling a more detailed evaluation of seismic risks across different fault segments and site classifications. This enhancement ensures a more localized and accurate hazard estimation, improving its applicability for engineering design, disaster mitigation planning, and strategic infrastructure development.

By integrating these improvements, this study provides a more comprehensive and site-specific seismic hazard assessment, ensuring that the updated PSHA model better reflects the complex fault interactions and geotechnical variations in MMR. The results emphasize the importance of local site effects, fault segmentation, and updated seismic source characterization in refining hazard models, contributing to better-informed risk assessments for future infrastructure projects.

3.4.5. Prospectus Area in MMR

The identification of potential CCS sites requires a multidisciplinary approach integrating geological stability, seismic hazard assessment, and regional land-use planning. The seismotectonic map (**Fig. 7**) provides critical information on active fault segments and structural geology, which influence subsurface stability. **Figures 10–12** illustrate PGA and PSA variations, offering insights into seismic risks at different probability levels (2% in 50 years and 7% in 75 years). Lower PGA and PSA regions may indicate areas with reduced seismic hazard, which is a crucial factor for CCS feasibility.

Based on the seismic hazard values for Malili and surrounding areas, PGA of 0.50 g, PSA S_s (0.2s) of 1.20 g, and PSA S_1 (1s) of 0.55 g at Site Class SB, these values are slightly below the SNI (2019) thresholds. However, due to the region's complex tectonic setting, especially the proximity to active fault systems near LM and the broader influence of the Palu-Koro fault system, we strongly recommend that infrastructure in this area adopt a Seismic Design Category D. This recommendation is particularly relevant for strategic infrastructure and critical facilities such as CCS, where structural resilience is essential to mitigate future seismic risks.

CCS suitability is also influenced by land-use policies and industrial development plans**.** The MMR has been identified as a prospective area for industrial expansion, including nickel processing and strategic infrastructure development, as outlined in the East Luwu Regency Long-Term Development Plan (PERDA Kabupaten Luwu Timur, 2005) and Indonesia's National Industrial Development Strategy**.** The presence of ultramafic rock formations further supports the potential for CO_2 mineralization and storage, aligning with national CCS policies.

Regulatory frameworks such as Ministerial Regulation, MEMR No. 2/2023, and Presidential Regulation No. 14/2024 establish legal provisions for CCS implementation in Indonesia. While Malili is not yet designated as an official CCS, its geological and industrial characteristics suggest that it may be considered for feasibility studies in the future. This study provides a geohazard and seismic risk assessment as an essential first step in evaluating the feasibility of strategic infrastructure projects, including CCS development, in the MMR.

4. Conclusions

This study presents a comprehensive seismotectonic and seismic hazard analysis of the MMR, integrating tectonic interpretations with quantitative ground motion assessments. The region exhibits significant seismic hazards, as indicated by complex fault mechanisms and elevated hazard parameters such as PGA and PSA values. These findings provide critical insights into the seismic character of the MMR, particularly within the MFZ and the LM corridor.

The analysis reveals that seismic risk in the area is spatially variable and strongly influenced by the distribution and interaction of active fault segments. Notably, the highest hazard values, PGA of up to 0.50 g, PSA at 0.2 seconds of 1.20 g, and PSA at 1.0 second of 0.5 g (for SB site class, with 2% probability of exceedance in 50 years), suggest the presence of localized zones of intense seismic potential. These results underscore the need for site-specific considerations in infrastructure development, especially for facilities with long operational lifespans and high safety demands such as CCS.

By integrating detailed hazard quantification and tectonic interpretation, this research contributes valuable data for regional seismic risk assessment and infrastructure planning. The calculated hazard parameters, while slightly below the thresholds of national standards, highlight the importance of applying appropriate seismic mitigation strategies in regions with complex fault systems. Given the intricate tectonic framework of the MMR, a conservative design approach remains essential to ensure the safety and long-term viability of critical infrastructure projects such as CCS. The findings emphasize not only the need for robust structural design but also for continuous monitoring and adaptive engineering practices to reduce seismic risk in this geodynamically active area.

Ultimately, this study demonstrates how seismotectonic and hazard analyses can serve as essential tools for informed decision-making in regional development planning. The integration of geological and engineering perspectives is vital to building resilient infrastructure in seismically vulnerable regions.

Acknowledgments

The authors thank the Geological Survey Center for funding the site survey within Research Mapping of the potential distribution of ultramafic materials in the Malili regions, Number 371. K/GL.04.BGS/2022. We also thank our Research Center for Geological Disaster, National Research and Innovation Agency (BRIN), and Seismotectonic Working Group colleagues in the Centre for Geological Survey, Geological Agency, Ministry of Energy, and the Mineral Resources Republic of Indonesia for supporting the completion of this scientific article.

References

Allen, T. I., & Wald, D. J. 2009. On the Use of High-Resolution Topographic Data as a Proxy for Seismic Site Conditions (VS30). Bulletin of the Seismological Society of America, 99(2A), 935–943. doi:10.1785/0120080255

Ali, A., Farid, A., Awan, U.F., Amin, Y., Zafar, W.A., Bangash, A.A., Ullah, S., 2023. Gravity survey to delineate the subsurface extension of the Khair-i-Murat Thrust under the Sub-Himalayas Kohat-Potwar region Pakistan. Himalayan Geology. 44(1), 117-129.

American Society of Civil Engineers, ASCE., 2010. Minimum Design Loads for Buildings and Other Structures, Structural Engineering Institute.

American Society of Civil Engineers (ASCE). (2016). Minimum design loads and associated criteria for buildings and other structures (ASCE 7-16). Reston, VA: ASCE Press.

Ansari, A., Azhoor, F., Rao, K, S., Jain, A, K.., 2022. Seismic hazard assessment studies based on deterministic and probabilistic approaches for the Jammu region, NW Himalayas, Arabian Journal of Geosciences, 151, 1081, doi.org/10.1007/s12517-022-10330-z.

Aromada, S. A., Eldrup, N. H., Øi, L. E., 2021. Capital cost estimation of CO_2 capture plant using Enhanced Detailed Factor (EDF) method: Installation factors and plant construction characteristic factors, International Journal of Greenhouse Gas Control, 110, 103394, doi.org/10.1016/j.ijggc.2021.103394, 2021.

Badan Meteorologi Klimatologi dan Geofisika, BMKG., 2019. Katalog Gempabumi Signifikan dan Merusak 1821 – 2018, Pusat Gempabumi dan Tsunami, first edition. Badan Meteorologi Klimatologi dan Geofisika, Jakarta.

Bazzurro, P and Cornell, C, A., 1999. Disagregation of Seismic hazard, Bulletin of the Seismological Society of America, 89, 2, 501-520.

Beaudoin, T., Bellier, O., Sebrier, M., 2003. Present-day stress and deformation fields within the Sulawesi Island area (Indonesia) Geodynamic Implications, Bulletin de la Société Géologique de France, 174 (3), 305–317, doi.org/10.2113/174.3.305, 2003.

Bellier, O., S´ebrier, M., Seward, D., Beaudouin, T., Villeneuve, M., Putranto, E., 2006. Fission Track and Fault Kinematics Analyses for New Insight Into the Late Cenozoic Tectonic Regime Changes in West-Central Sulawesi (Indonesia), Tectonophysics, 413 (3-4), 201–220, doi.org/10.1016/j.tecto.2005.10.036

Bergman, S.C., Coffield, D.Q., Talbot, J.P., Garrard, R.A., 1998. Tertiary Tectonic Evolution of Sulawesi and the Makassar Straits, Indonesia: evidence for a Miocene continent-continent collision, Geological Society, 106, 391 – 429, doi.org/10.1144/GSL.SP.1996.106.01.25, 1998.

Blakely, R.J., 1996. Potential Theory in Gravity and Magnetic Applications, Cambridge University Press.

Boore, D. M., Joyner, W. B., & Fumal, T. E. 1997. Equations for Estimating Horizontal Response Spectra and Peak Acceleration from Western North American Earthquakes: A Summary of Recent Work, Seismological Research Letters, 68(1), 128–153. doi:10.1785/gssrl.68.1.128

Bredesen, K., 2022. Assessing rock physics and seismic characteristics of the Gassum Formation in the Stenlille aquifer gas storage – A reservoir analog for the Havnsø CO_2 storage prospect, Denmark, Earthq. Spectra, 30(3), 1057–1085, International Journal of Greenhouse Gas Control. 114. 103583, doi.org/10.1016/j.ijggc.2022.103583

Brian, S., Chiou, J., Youngs, R., R., 2014. Update of the Chiou and Youngs NGA Model for the Average Horizontal Component of Peak Ground Motion and Response Spectra, SAGA Journal, 30(3), doi.org/10.1193/072813EQS219M, 2014.

Brian, S., Chiou, J., Young, R., R., 2006. Chiou and Young PEER-NGA Empirical Ground Motion Model for the Average Horizontal Component of Peak Acceleration, and Pseudo-Spectral Acceleration for Spectral Periods of 0.01 to 10 seconds, Interim Report for USGS Review.

Building Seismic Safety Council, BSSC, 1997. NEHRP Recommended Provisions for Seismic Regulations for New Buildings and Other Structures, Part 1. FEMA 302, Washington.

Chen, W-P., Molnar, P. 1983. Focal depths of intracontinental and intraplate earthquakes and their implications for the thermal and mechanical properties of the lithosphere. Journal of Geophysical Research, https://doi.org/10.1029/JB088iB05p04183

Cheng, Y., Liu, W., Xu, T., Zhang, Y., Zang, X., Xing, Y., Feng, B., Xia, Y., 2023. Seismicity induced by geological CO_2 storage: A Review, Earth-Science Reviews. https://doi.org/10.1016/j.earscirev.2023.104369

Cipta, A., Robiana, R., Griffin, J.D., Horspool, N., Hidayati, S., Cummins, P., 2016. A probabilistic seismic hazard assessment for Sulawesi, Indonesia. Geohazards in Indonesia: Earth Science for Disaster Risk Reduction, Geological Society, London, Special Publication, 441, doi.org/10.1144/SP441.6, 2016.

Chiou, B. and Young, R., 2014. Update of the Chiou and Youngs NGA model for the average horizontal component of peak ground motion and response spectra, Earthquake Spectra, 30(3), 1117–1153, https://doi.org/10.1193/072813eqs219m

Coffield, D.Q., Bergman, S.C., Gerrard, R.A., Guritno, N., Robinson N.M., Talbot, J., 1993. Tectonic and stratigraphic evolution of the Kalosi PSC Area and associated development of a Tertiary petroleum system. South Sulawesi, Indonesia, Indonesian Petroleum Association, Proceedings 22nd Annual Convention Jakarta, 1, 679–706, 1993.

Djiada, I. 2024. PEP Donggi-Matindok Field mulai bor sumur TDG-001 di Kabupaten Morowali Utara. Banggai Raya. https://banggairaya.id/pep-donggi-matindok-field-mulai-bor-sumur-tdg-001-di-kabupaten-morowali-utara/

Escuder-Viruete, J., Fernandez, F, J., Valera, F. P., McDermott, F., 2024. Active Tectonics, Quaternary Stress Regime Evolution and Seismotectonic Faults in Southern Central Hispaniola: Implications for the Quantitative Seismic Hazard. Assessment, Geochemistry, Geophysics, Geosystems. 10.1029/2023GC011003, https://doi.org/10.1029/2023GC011003.

Frankel, A., 1995. Mapping seismic hazard in the central United States. Seismological Research Letters, 66(4), 8-21. https://doi.org/10.1785/BSSA0850031246

Global Centroid Moment Tensor, GCMT, 2022. Global CMT Catalog Search. Retrieve February 2, 2022, from https://www.globalcmt.org/CMTsearch.html.

GEM., 2018. The OpenQuake-engine User Instruction Manual Version 3.1.0, Global Earthquake Model (GEM), doi: 10.13117/GEM.OPENQUAKE.MAN.ENGINE.3.1.0, 198 page.

Gutenberg, B. and Richter, C.F., 1944. Frequency of Earthquakes in California. Bulletin of the Seismological Society of America, 34, 185-188.

International Seismological Centre Bulletin, ISC., 2020. Focal Mechanism Search. Retrieved February 8, 2020 from http://www.isc.ac.uk/iscbulletin/search/fmechanisms/interactive/, 2022.

Irsyam, M., Cummins, M., Asruifak, P.R., Faizal, M., Faizal, L., Natawidjaja, D.H., Widyantoro, S., Meilano, I., Triyoso, Rudiyanto, W. A., Hidayati, S., Ridwan, M., Hanifa, N.R., Syahbana, A.J., 2020. Development of the 2017 national seismic hazard maps of Indonesia, Earthquake Spectra 1-25, doi.org/10.1177/8755293020951206, 2020.

Jing, J., Tang, Z., Yang, Y., Ma, L., 2019. Impact of formation slope and fault on CO2 storage efficiency and containment at the Shenhua CO2 geological storage site in the Ordos Basin, China, International Journal of Greenhouse Gas Control, 88, 209-225. doi.org/10.1016/j.ijggc.2019.06.013.

Jorjiashvili, N., Gigiberia, M., Shengelia, I., Otinashvili, M., 2018. Integration of Geophysical and Geotechnical Soil Characteristics for Local Site Seismic Design in Georgia, Open Journal of Earthquake Research, 7(2), 108-123, doi.org/10.4236/ojer.2018.72007.

Kadarusman, A., Miyashita, S. Maruyama, S., Parkinson, C.D., Ishikawa, A., 2004. - Petrology, geochemistry and paleogeographic reconstruction of the East Sulawesi Ophiolite, Indonesia, Tectonophysics, 392(1-4), 55–83, doi.org/10.1016/j.tecto.2004.04.008.

Kaklamanos, J., Boore, D.M., Thompson, E.M., Campbell, K.W., 2011. Implementation of the Next Generation Attenuation (NGA) Ground-Motion Prediction Equations in FORTRAN and R. USGS.

Katili, J. A., 1991. Tectonic evolution of eastern Indonesian and its bearing on the occurrence of hydrocarbons, Marine and Petroleum Geology, 8(1), 70-83, doi.org/10.1016/0264-8172(91)90046-4.

Kim, M-C., Gihm, Y, S., Jeong, R-Y., Shinn, Y, J., Son, M., 2020. Site selection and characterization for onshore 10,000-ton-class CO_2 pilot storage in Early Miocene Janggi Basin, SE Korea: Storage potential and structural stability of siliciclastic-volcaniclastic storage combination, International Journal of Greenhouse Gas Control, 103, 103174 doi.org/10.1016/j.ijggc.2020.103174, doi.org/10.1016/j.ijggc.2020.103174.

Liu, C. S., and Wang, C. W., 2015. Earthquake Barcode from a Single-Degree-of-Freedom System, Natural Science, 7(1), 18-31, doi.org/10.4236/ns.2015.71003.

Mai, P.M., Spudich, P., Boatwright, J., 2005. Hypocenter Locations in Finite-Source Rupture Models, Bulletin of the Seismological Society of America, 95(3), 965-980, doi.org/10.1785/0120040111, 2005.

McGuire, R. K. 1995. Probabilistic seismic hazard analysis and design earthquakes: Closing the loop. Bulletin of the Seismological Society of America, 85(5), 1275–1284. https://doi.org/10.1785/BSSA0850051275

Ministry of Energy and Mineral Resources Regulation (MEMR). 2023. Regulation on the Implementation of CCS (Carbon Capture and Storage) and CCUS (Carbon Capture, Utilization and Storage) in Upstream Oil and Gas Business Activities. Regulation No. 2. https://jdih.esdm.go.id/dokumen/view?id=2371.

Ministry of Public Works and Housing, MPWH., 2017. Peta Sumber dan Bahaya Gempa Indonesia, Kementerian PUPR, Jakarta.

Mirnanda, E., Siagian, H. P., 2007. Peta Anomali Bouguer Lembar Malili Sulawesi, Pusat Survei Geologi, Bandung.

Molnar, P., & Chen, W. (1983). Focal depths of intracontinental and intraplate earthquakes and their implications for the thermal and mechanical properties of the lithosphere. Geophysical Journal International, 75(2), 457-488. https://doi.org/10.1111/j.1365-246X.1983.tb05059.x

Moratto, L., Santulin, M., Tamaro, A., Sarao, A., Vuan A., Rebez, A., 2023. Near-source ground motion estimation for assessing the seismic hazard of critical facilities in central Italy, Bulletin of Earthquake Engineering, 21, 53-57 doi.org/10.1007/s10518-022-01555-0.

National Earthquake Hazards Reduction Program (NEHRP). 2020. Recommended seismic provisions for new buildings and other structures. Federal Emergency Management Agency (FEMA) Report P-2082

Nazarinezhad, Z., Sepahvand, M., Nasrabadi, A., 2024. Seismotectonic investigation in northwest Zagros, Iran: Analysis of Ezgeleh Mw 7.3 aftershocks. J Seismol, 28, 81-101, doi.org/10.1007/s10950-023-10184-2.

Nugraha, A. M. S., Hall, R., Boudagher-Fadel, M., 2022. The Celebes Molasse: A revised Neogene stratigraphy for Sulawesi, Indonesia.Journal of Asian Earth Sciences, 228, 105140. https://doi.org/10.1016/j.jseaes.2022.105140

Nugraha, A. M. S., Adhitama, R., Switzer, A. D., & Hall, R. 2023. Plio-Pleistocene sedimentation and palaeogeographic reconstruction in the Poso Depression, Central Sulawesi, Indonesia: From a sea channel to a land bridge. Journal of Palaeogeography, 12(3), 331–357. https://doi.org/10.1016/j.jop.2023.05.003

Pagani, M., Monelli, D., Weatherill, G., Danciu, I., Crowley, H., Silva, V., Henshaw, P., Butler, L., Nastasi, M., Panzer, L., Simionato, M., Vigano, D., 2014. OpenQuake engine: An open hazard (and risk) Software for the Global Earthquake Model, Seismol. Res. Lett. 85(3), 692–702, doi.org/10.1785/0220130087.

Patria, A., Natawidjaja, D. H., Daryono, M.R., Hanif, M., Puji, A.R., Tsutsumi, H., 2023. Tectonic landform and paleoseismic events of the easternmost Matano fault in Sulawesi, Indonesia, Tectonophysiscs, 852 (2023) 229762. https://doi.org/10.1016/j.tecto.2023.229762

Parkinson, C., 1998a. An outline of the petrology, structure and age of the Pompangeo Schist Complex of central Sulawesi, Indonesia, Island Arc, 7(1-2), 231–245, doi.org/10.1046/j.1440-1738.1998.00171.x, 1998a.

Parkinson C., 1998b. Emplacement of the East Sulawesi Ophiolite: evidence from subophiolite metamorphic rocks, Journal of Asian Earth Sciences, 16(1), 13–28, doi.org/10.1016/S0743-9547(97)00039-1.

Parkinson, C. D., Miyazaki, K., Wakita, K., Barber, A. J., Carswell, D. A., 1998. An Overview and Tectonic Synthesis of the pre-Tertiary very-high-pressure Metamorphic and Associated

Rocks of Java, Sulawesi and Kalimantan, Indonesia. Island Arc. 7(1-2), 184–200, doi.org/10.1046/j.1440-1738.1998.00184.x, 1998.

Peraturan Daerah (PERDA) Kabupaten Luwu Timur Nomor 2 Tahun 2005. Tentang Rencana Pembangunan Jangka Panjang (RPJP) Kabupaten Luwu Timur. Regional Regulation of East Luwu Regency Number 2 of 2005. Concerning the Long-Term Development Plan (RPJP) of East Luwu Regency.

Permatasari, A. W., Santoso, D., Setianingsih., 2019. Subsurface Modelling Based on Gravity Data of Rendingan–Ulubelu–Waypanas (RUW) Geothermal Field, Lampung, Indonesia, IOP Conference Series and Environmental Science, 318, 012002, doi.org/10.1088/1755-1315/318/1/012002.

Petersen, M, D., Shumway, A, M., Powers, P, M., Mueller, C, S., Moschetti, M, P., Frankel, A, D., Rezaeian S., McNamara, D, E., Luco, N., Boyd, O, S., Rukstales, K, S., Jaiswal, K, S., Thompson, E, M., Hoover, S, M., Clayton, B, S., Field, E, H., Zeng, Y. 2019. The 2018 update of the US National Seismic Hazard Model: Overview of model and implications. Earthquake Spectra. 1, 37. https://doi.org/10.1177/87552930198781

Pettersson, M, D., Moschetti, M, P., Powers, P, M., Mueller, C, S., Haller, K, M., Frankel, A, D., Zeng, Y., Rezaeian, S., Harmsen, S, C., Boyd, O, S., Field, N., Chen, R., Rukstales, K, S., Luco, N., Wheeler, R, L., Williams, R, A., Olsen, A, H. 2014. Documentation for the 2014 Update of the United States National Seismic Hazard Map, U.S. Geological Survey Open-File Report 2014-1091, https://doi.org/10.3133/ofr20141091

Pettersson, P., Tveit, S., Gasda, S, E., 2022. Dynamic estimates of extreme-case CO2 storage capacity for basin-scale heterogeneous systems under geological uncertainty, International Journal of Greenhouse Gas Control, 116, 103613, doi.org/10.1016/j.ijggc.2022.103613

Pirttijärvi, M., 2004. Grablox User's Guide Version 1.5. Geological Survey of Finland, Espoo.

Presidential Regulation. 2024. Decision No. 14/2024. Penyelenggaraan Kegiatan Penangkapan dan Penyimpanan Karbon.

Pusat Survey Geologi (PSG). 2022a. Pemetaan Batuan Ultramafik untuk Carbon Storage di Daerah Malili dan Sekitarnya, Kabupaten Luwu Timur, Provinsi Sulawesi Selatan. Badan Geologi, Kementerian Energi dan Sumber Daya Mineral. Unpublished Report.

Pusat Survey Geologi (PSG). 2022b. Pemetaan Batuan Ultramafik untuk Carbon Storage di Daerah Soroako dan Sekitarnya, Kabupaten Luwu Timur, Provinsi Sulawesi Selatan. Badan Geologi, Kementerian Energi dan Sumber Daya Mineral. Unpublished Report.

Pusat Survey Geologi,, 2022. Pemetaan Batuan Ultramafik Untuk Carbon Storage di Daerah Soroako dan Sekitarnya, Kabupaten Luwu Timur, Provinsi Sulawesi Selatan, Badan Geologi, Kementerian Energi dan Sumber Daya Minesal, Unpublished Final Report.

Rasool, M. H., Ahmad, M., & Ayoub, M. 2023. Selecting Geological Formations for CO2 Storage: A Comparative Rating System. Sustainability, 15(8), 6599. https://doi.org/10.3390/su15086599

Rudman, A., Dauglas, J., Tubaldi, E., 2024. The assessment of probabilistic seismic risk using ground-motion simulations via a Monte Carlo approach. Natural Hazards, 120, 6833-6852, doi.org/10.1007/s11069-024-06497-1.

Scherbaum, F., Cotton, F., Smit, P., 2004. On the Use of Response Spectral-Reference Data for the Selection and Ranking of Ground-Motion Models for Seismic-Hazard Analysis in Region of Moderate Seismicity: The Case of, Rock Motion, Bulletin of the Seismological Society of America, 94(6), 2164-2185, doi.org/10.1785/0120030147, 2004.

Scordilis, E., M. 2006. Empirical global relations converting *Ms* and *mb* to moment magnitude. Journal of Seismology 10: 225-236. DOI: 10.1007/s10950-006-9012-4

Sianko, I., Ozdemir, Z., Khoshkholgi, S., Garcia, R., Hajirasouliha, I., Yazgan, U., Pilakoutas, K., 2020. A practical probabilistic earthquake hazard analysis tool: case study Marmara region, Bulletin of Earthquake Engineering18, 2523-2555, doi.org/10.1007/s10518-020-00793-4.

Simanjuntak, T, O., and Barber, A. J., 1996. Contrasting tectonic styles in the Neogene orogenic belts of Indonesia, Geological Society Publication, 106, 185-201, doi.org/10.1144/GSL.SP.1996.106.01.12, 1996.

Simanjuntak, T, O., Rusmana, E., Surono, Supandjono, J, B., 2007. Geologic Map of Malili Quadrangale, North Sulawesi, Scale 1:250.000, Center for Geological Survei, Geological Agency, Bandung.

Somerville, P. G., Smith, N. F., Graves, R. W., & Abrahamson, N. A. 1997. Modification of empirical strong ground motion attenuation relations to include the amplitude and duration effects of rupture directivity.Seismological Research Letters, Vol 68, No. 1, https://doi.org/10.1785/gssrl.68.1.199

Standar Nasional Indonesia, SNI, 2016. SNI 2833:2016 Perencanaan Jembatan terhaap Beban Gempa, Badan Standarisasi Nasional.

Standar Nasional Indonesia, SNI, 2019. SNI 1726:2019 Tata cara perencanaan ketahanan gempa untuk struktur bangunan gedung dan non Gedung, Badan Standarisasi Nasional.

Sycheva, N, A., 2024. Seismicity And Crustal Seismotectonic Deformations of The Anatolian Plate (Turkey), Geodynamics and Tectonophysics, 15, 1, 0743, https://doi:10.5800/GT-2024-15-1-0743

United States Geological Survey Earthquake Catalog, USGSEC., 2022. Search Earthquake Catalog, Retrieved March 12, 2020 from https://earthquake.usgs.gov/earthquakes/search/, 2022.

Vavlas, N., Kiratzi, A., Margaris, B., Karakaisis, G., 2019. Probabilistic Seismic Hazard Assessment (PSHA) for Lesvos Island using the Logic Tree Approach, Bulletin of the Geological Society of Greece, 55,109-136, http://dx.doi.org/10.12681/bgsg.20705.

Villeneuve, M., Gunawan, W., Cornee, J-J., Vidal, O., 2002. Geology of the central Sulawesi belt (eastern Indonesia): Constraints for geodynamic models, International Journal of Earth Sciences, 91, 524-537, doi.org/10.1007/s005310100228, 2002.

Wahyudi, E.J., Kynantoro, Y., Alawiyah, S, 2017. Second Vertical Derivative Using 3-D Gravity Data for Fault Structure Interpretation, IOP Conference Series Journal of Physics 877, 012039, doi.org/10.1088/1742-6596/877/1/012039, 2017.

Watkinson, I.M., and Hall, R., 2017. Fault systems of the eastern Indonesian triple junction: Evaluation of Quaternary activity and implications for seismic hazards. In: Cummins, P.R., Meilano, I. (Eds.), Geohazards in Indonesia: Earth Science for Disaster Risk Reduction. Geological Society of London, London, pp. 71–120. https://doi.org/10.1144/SP441.8.

Wells, D, L., and Coppersmith, K, J., 1994. New Empirical Relationships among Magnitude, Rupture Length, Rupture Width, Rupture Area, and Surface Displacement, Bulletin of the Seismological Society of America, 84(4), 974-1002, doi.org/10.1785/BSSA0840040974, 1994.

Weichert, D. H. 1980. Estimation of the earthquake recurrence parameters for unequal observation periods for different magnitudes. Bulletin of the Seismological Society of America, 70(4), 1337–1346. doi.org/10.1785/BSSA0700041337

Wesnousky, S, G., 1988. Seismological and Structural Evolution of Strike-Slip Faults, Nature, Vol 335. Doi: 10.1038/335340a0

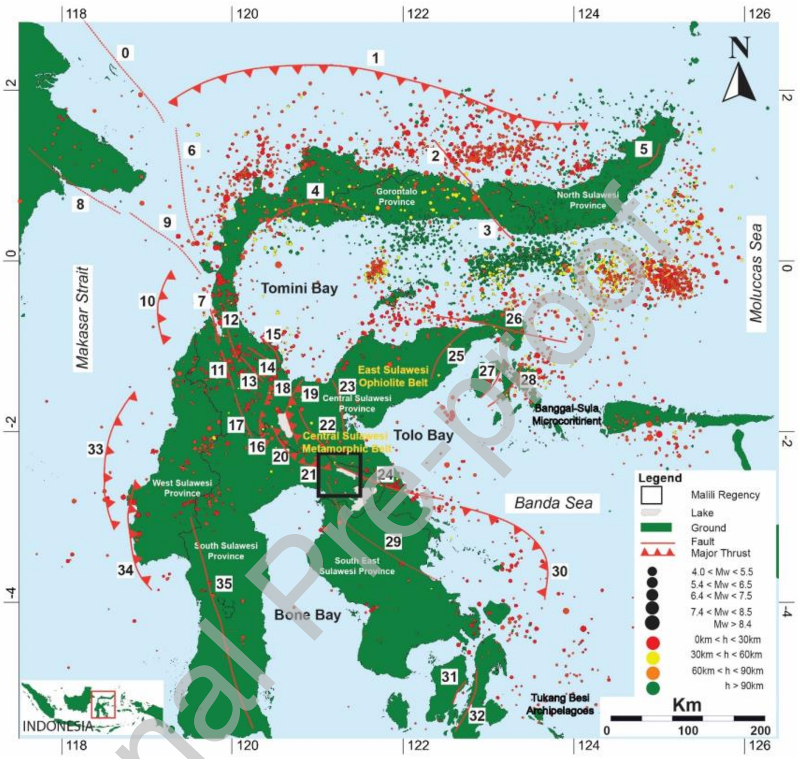

Fig. 1. Distribution of major thrusts and faults around Sulawesi, the number on the map represents the faults and major thrusts (Sukamto et al., 1994; Simanjuntak, 2007; Simons et al., 2007; Sukamto, 2012; Pagani et al., 2014). Major thrusts and faults represented as numbers in the white box are defined in Table 1. Spatial distribution of earthquake events, data collected from 3 main well-known online global catalogs: the Global Centroid Moment Tensor Project (GCMT, 2022), the United States Geological Survey Earthquake Catalog (USGSEC, 2022), and the International Seismological Centre (ISC, 2020) since the local data agency was not sufficient. Statistical data results range from the years 1907-2022 and cover a wide range of magnitudes ($4.4 \leq Mw \leq 8.1$, $3.0 \leq Mb \leq 6.7$, $4.1 \leq Ms \leq 7.7$) and depths (1 to 640 km). Data are filtered from duplicates and sorted by the best review, and the relocation process has refined some data. The data found 6334 records, including 697 data from GCMT and 1167 data from ISC, and they are filtered to 5313 records from USGSEC (2022), GCMT (2022), and ISC (2020).

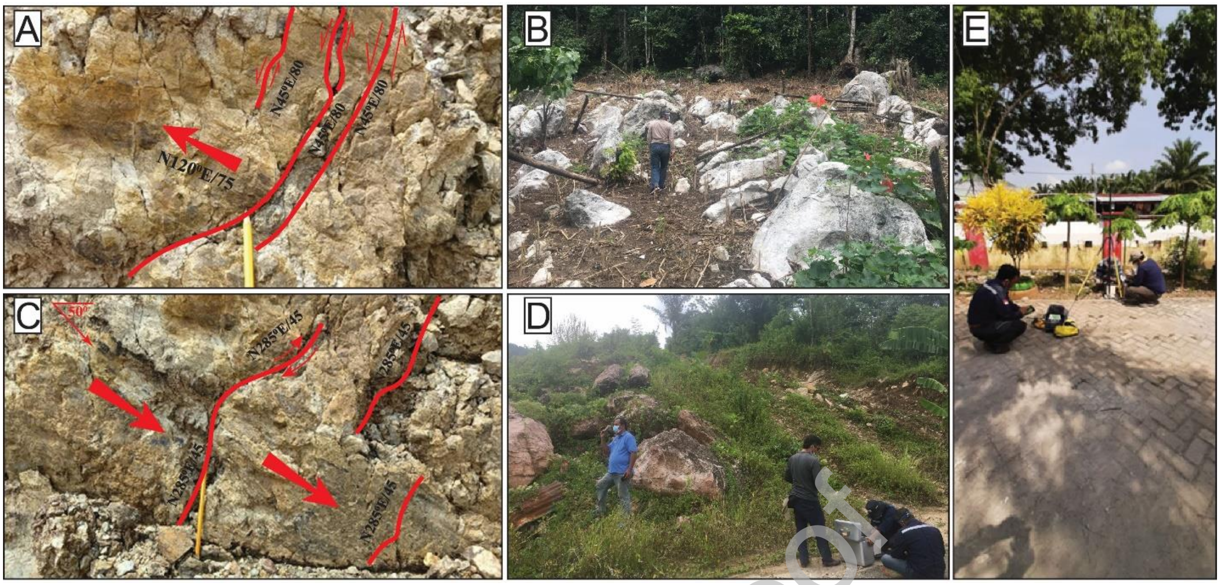

Fig. 2. (A) Illustrates a combination of shear and tension fractures in an outcrop of the MFZ near LM, showcasing its left-lateral strike-slip fault kinematics. (B) an outcrop of the Ultrabasic Complex is shown, revealing a mix of lithologies, including crystalline limestone. (C) displays another outcrop of the MFZ within Malili Regency, where a combination of shear and tension fractures suggests oblique normal fault kinematics. (D) depicts an outcrop of the Tomata Formation, characterized by sandstone and conglomerates. (E) Field activity of geophysical data acquisition of anomaly gravity. **The locations of these outcrops are indicated in Fig. 7.**

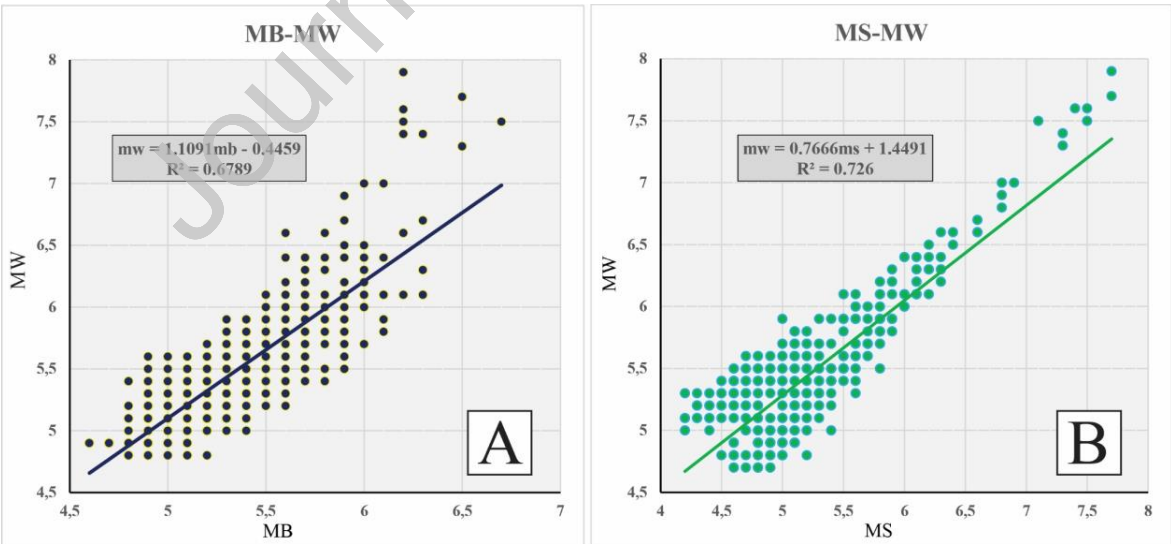

Fig. 3. (A) The black dots represent MB-MW scatter data, and the black line is the trendline equation of the MB-MW relationship **(B)** Green spots denote the MW and MS data, and the green line represents the relationship of MW-MS.

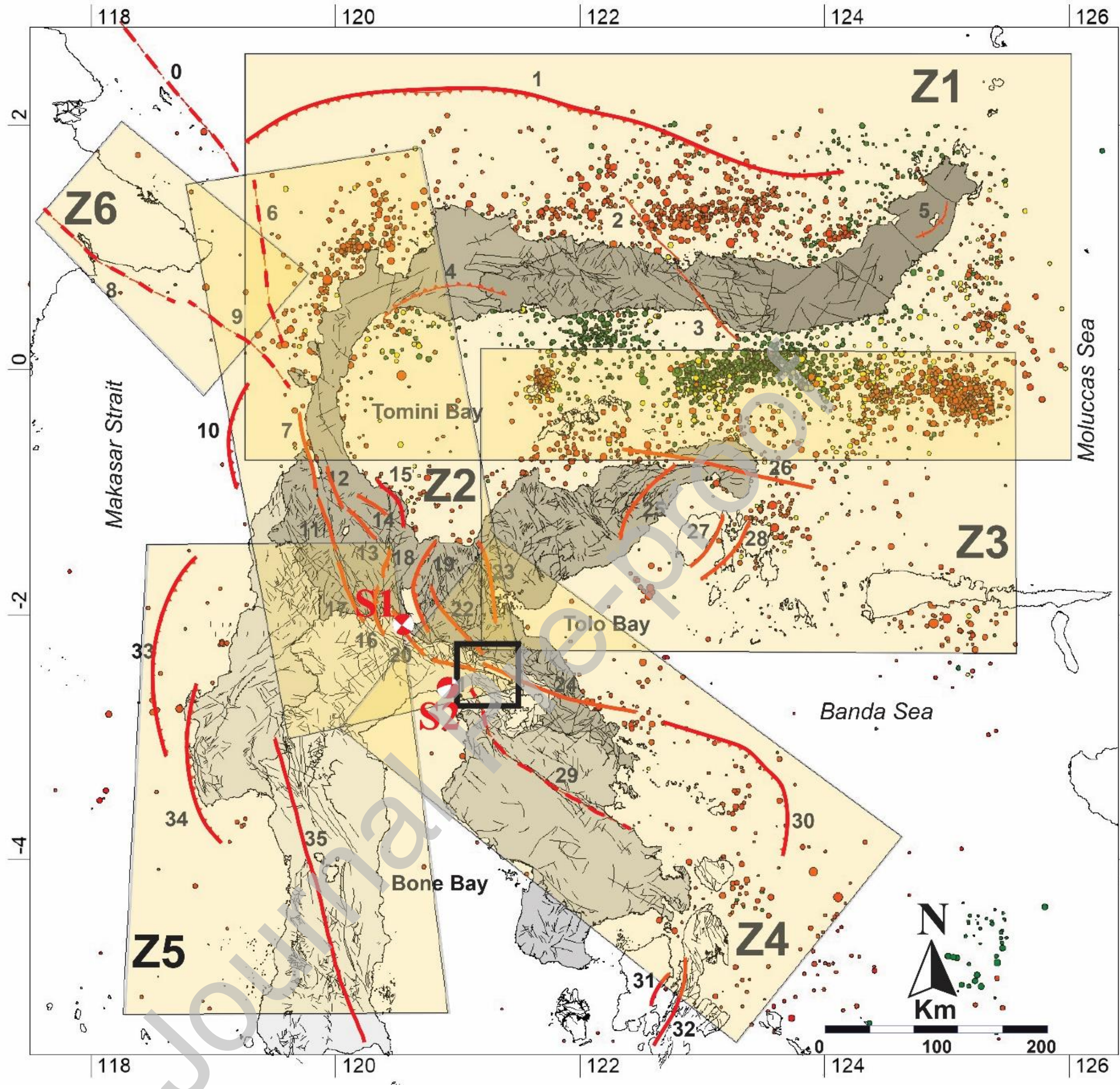

Fig. 4. The box describes the zonation of fault sources and the area of interest with a black frame that overlays Z2, Z3, and Z4. Two historical records, S1 and S2, with a magnitude of Mw 4.7 (S1) and Mw 5.6 (S2), occurred close to the MFZ and Malili Regency.

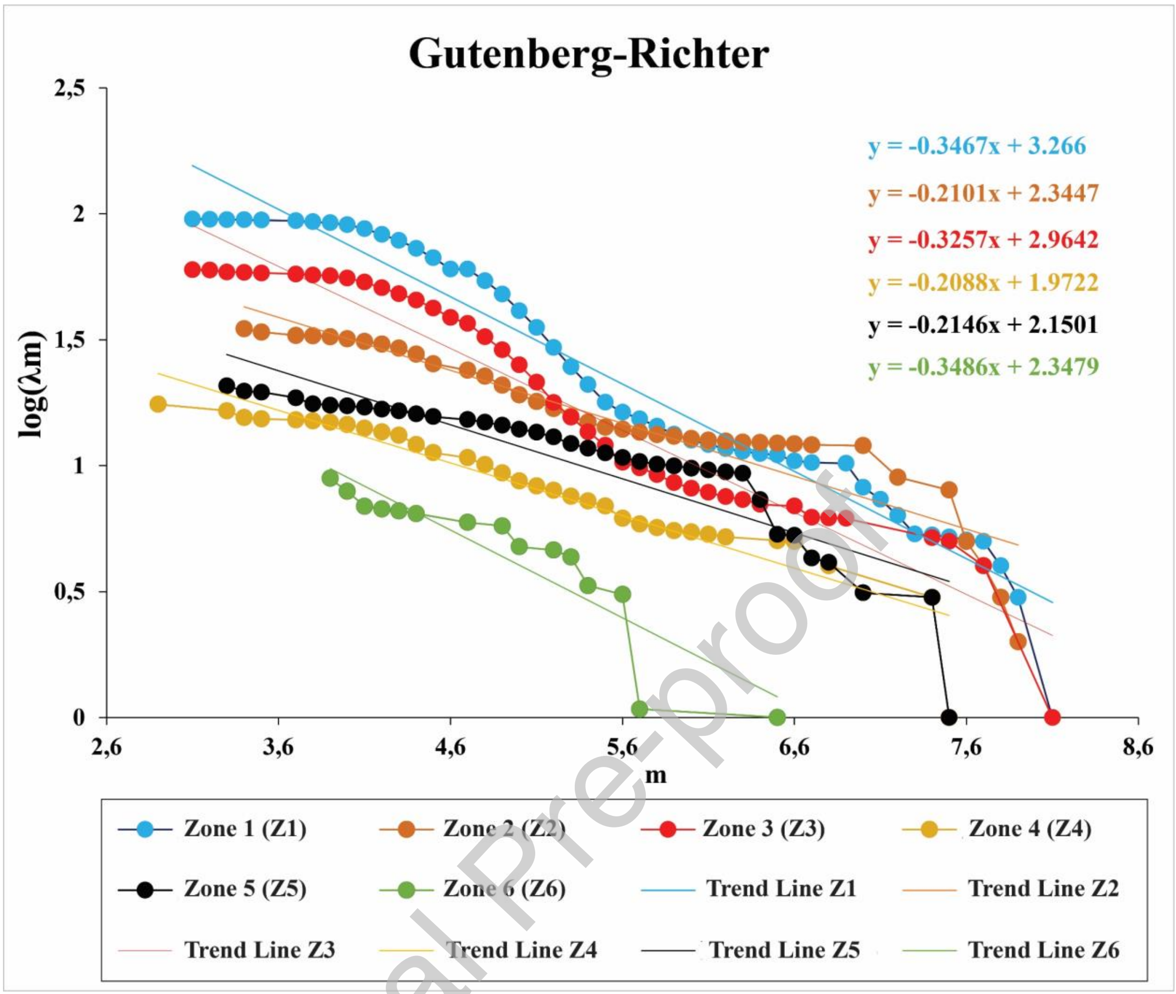

Fig. 5. The blue dots correspond to applying Gutenberg-Richter's Law in Zone Z1. The equation for this zone provides values of a=3.266 and b=0.3467. The other points and their equations for zones Z2-Z6 also adhere to Gutenberg-Richter's Law.

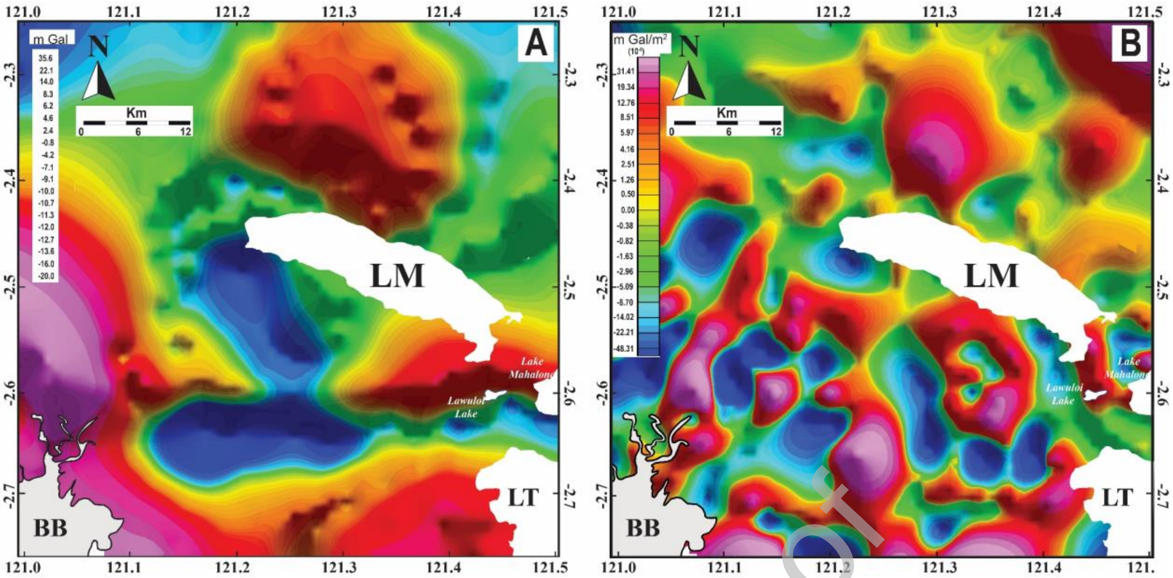

Fig. 6. (A) The residual anomaly map illustrates the spatial distribution of rock density in the lower part of the ground surface, indicating that a basin with low density characterizes the southern region of the LM (B). The analysis of the SVD anomaly gravity map of the LM region.

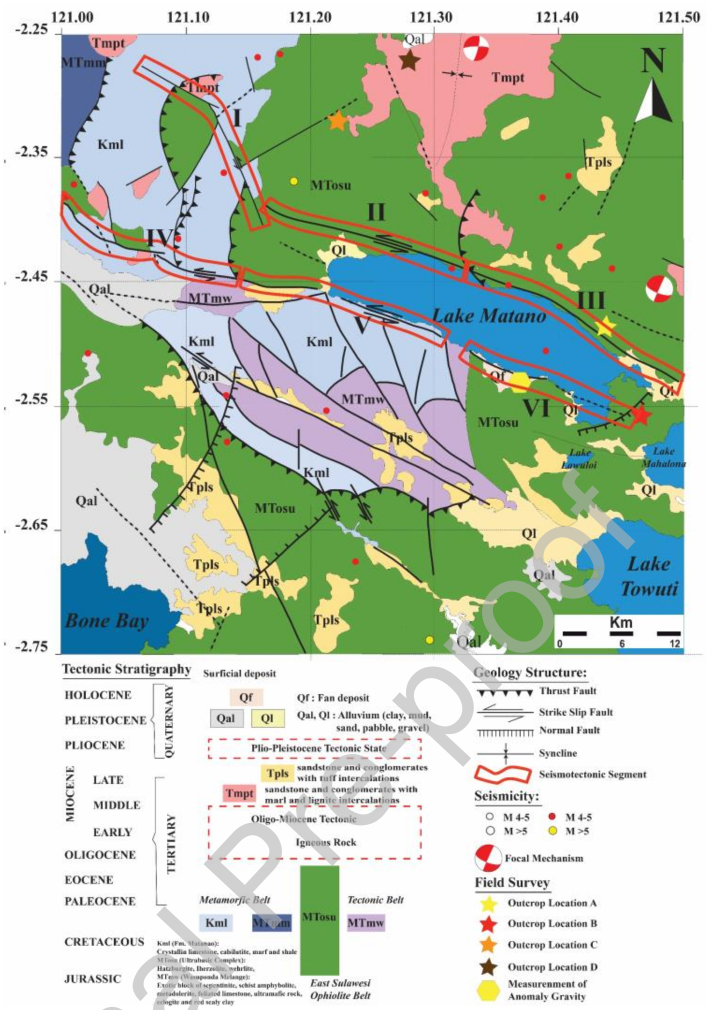

Fig. 7. The Seismotectonic Map of the Malili Regency shows major tectonic features and the distribution of earthquake Mw> 4.5. It can be interpreted as six seismotectonic segments based on structure and stratigraphy.

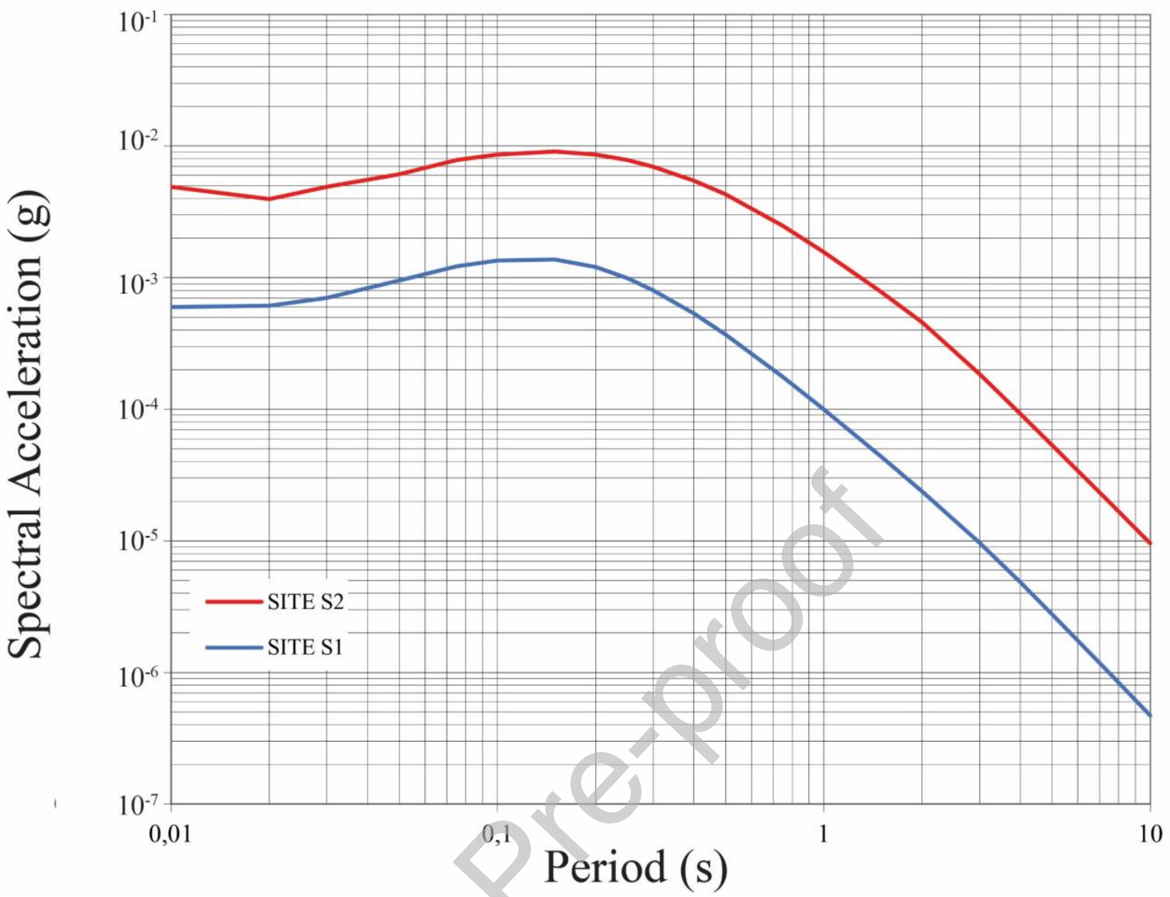

Fig. 8. PGA and 5% Damped PSA for site S1 (Mw=4.7) and Site S2 (Mw=5.6)

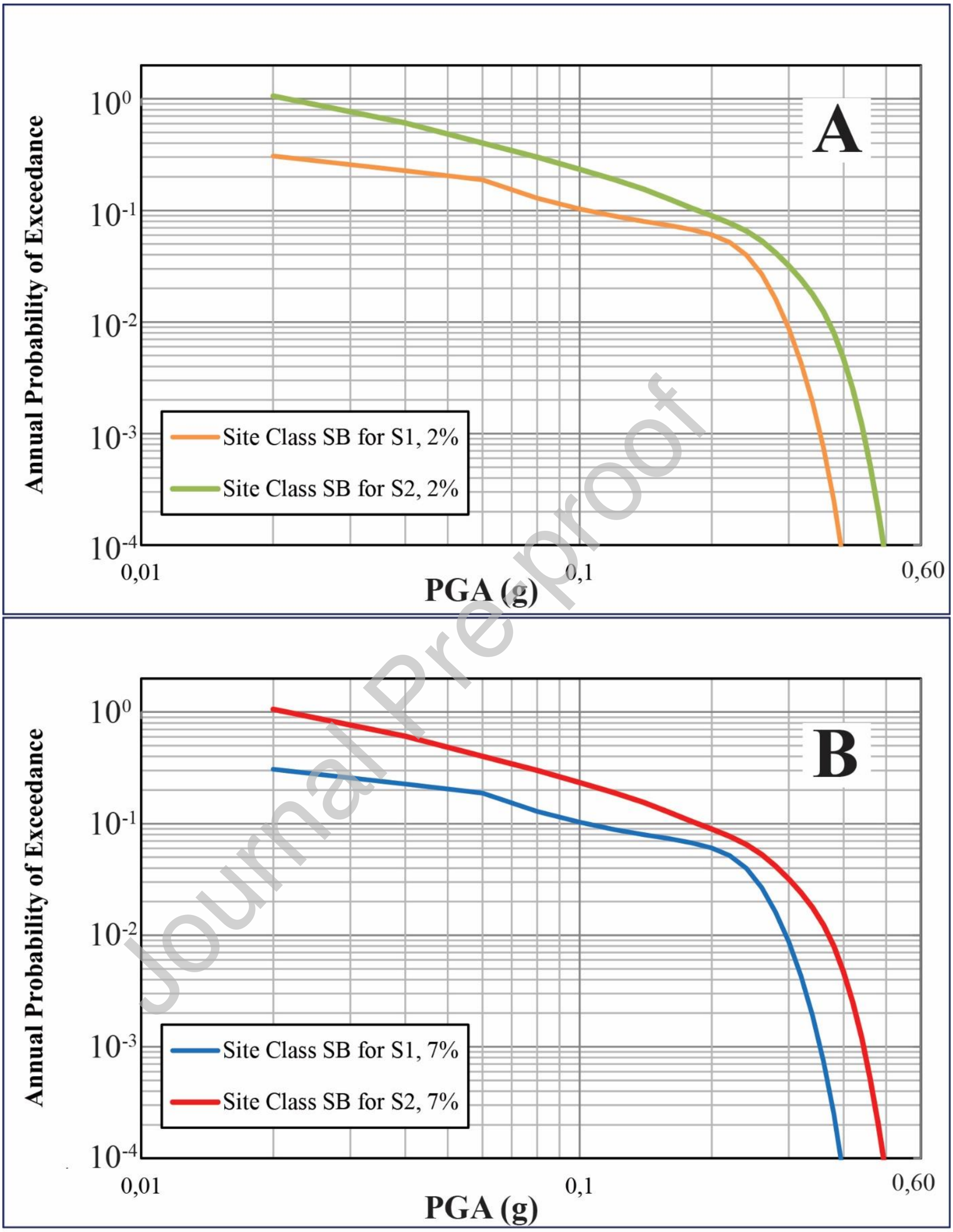

Fig. 9. (A) Hazards curves Site Class SB for Site S1 and S2, 2% probability in 50 years (2500 Return Period). (B) Hazards curves Site Class SB for sites S1 and S2, 7% probability in 75 years (1000 years).

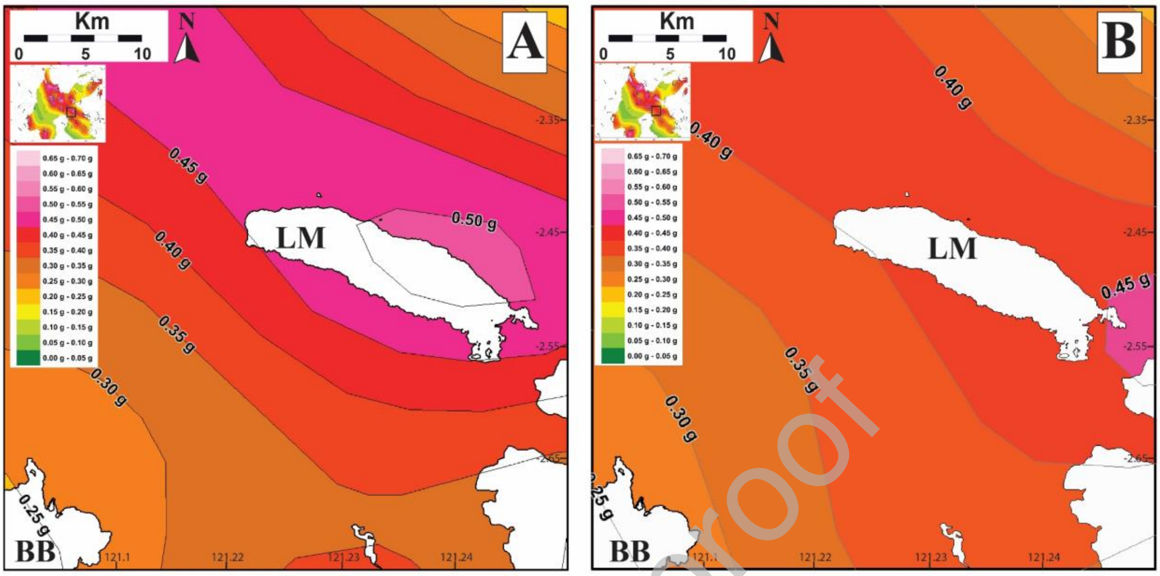

Fig. 10. (A) presents the PGA map for the MCE$_R$ with a 2% probability of exceedance in 50 years (2500-year return period) for site class Vs30 SB, while (B) shows the PGA map for the MCE$_R$ with a 7% probability of exceedance in 75 years (1000-year return period).

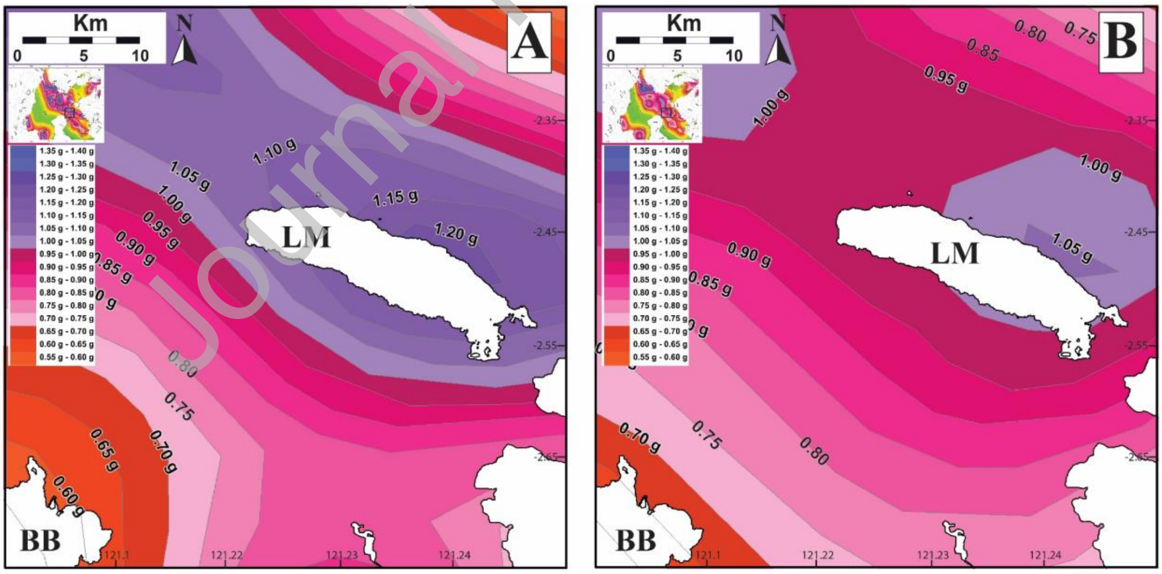

Fig. 11. The 5% damped PSA maps for short periods (SS) of 0.2 seconds. (A) shows the PSA map for a 2% probability of exceedance in 50 years (2500-year return period), and (B) displays the PSA map for a 7% probability of exceedance in 75 years (1000-year return period), both for site class Vs30 SB.

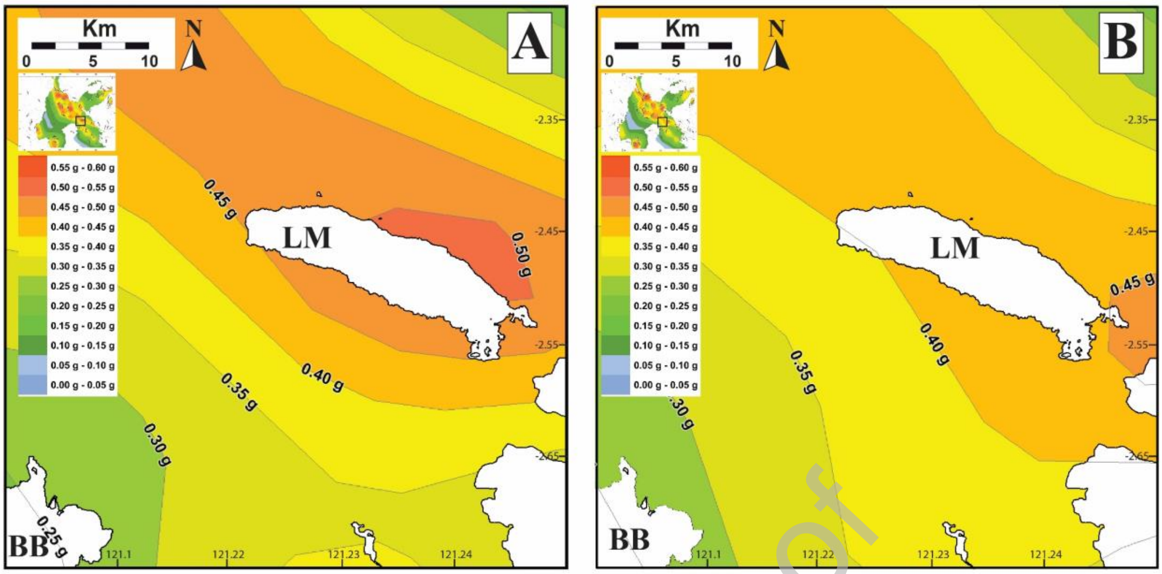

Fig. 12. The 5% damped PSA maps for long periods (S1) of 1.0 seconds. (A) presents the PSA map for a 2% probability of exceedance in 50 years (2500-year return period), while (B) shows the PSA map for a 7% probability of exceedance in 75 years (1000-year return period), both for site class Vs30 SB.

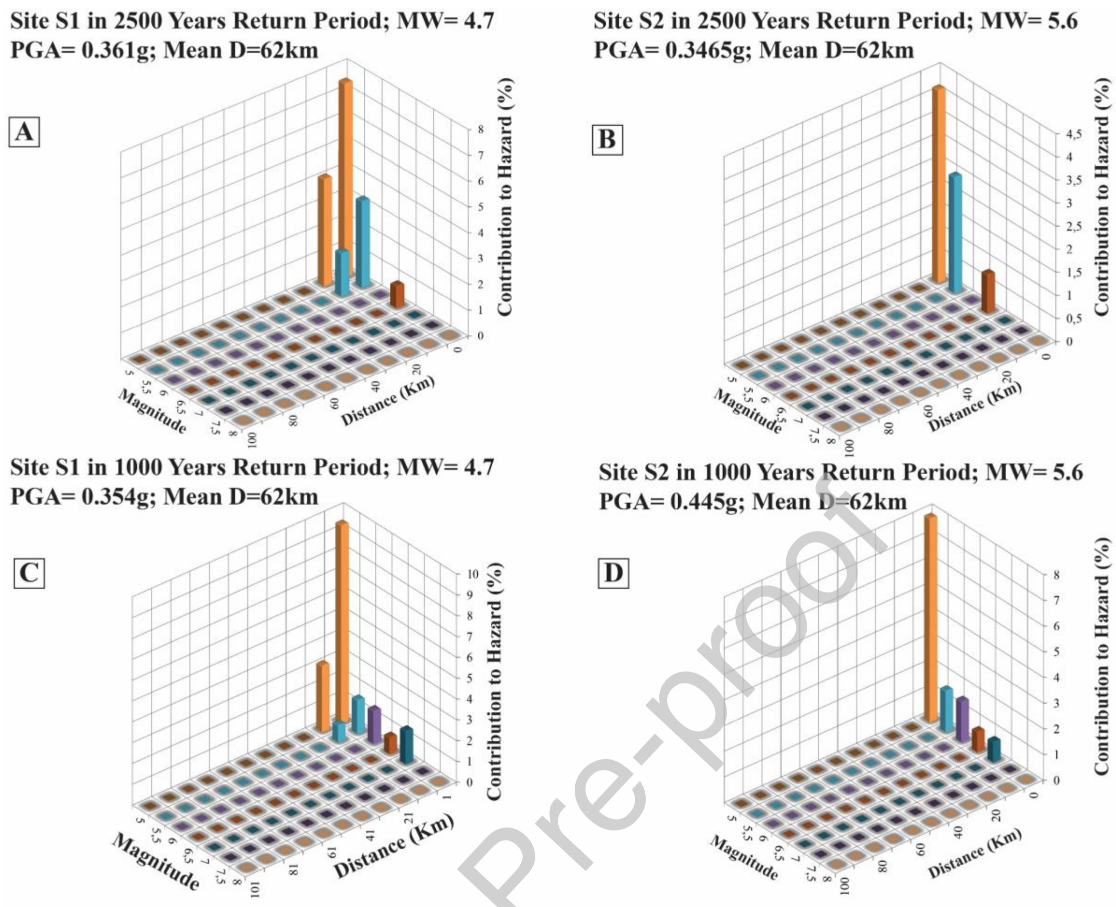

Fig. 13. Disaggregation chart depicting the relative contribution of different magnitude and distance ranges to the hazard. (A) Site S1 in 2500years return period; MW=4.7, PGA=0.361g; Mean D=62km. (B) Site S2 in 2500years return period; MW=5.6, PGA=0.3465g; Mean D=62km. (C) Site S1 in 1000years return period; MW=4.7, PGA=0.354g; Mean D=62km.

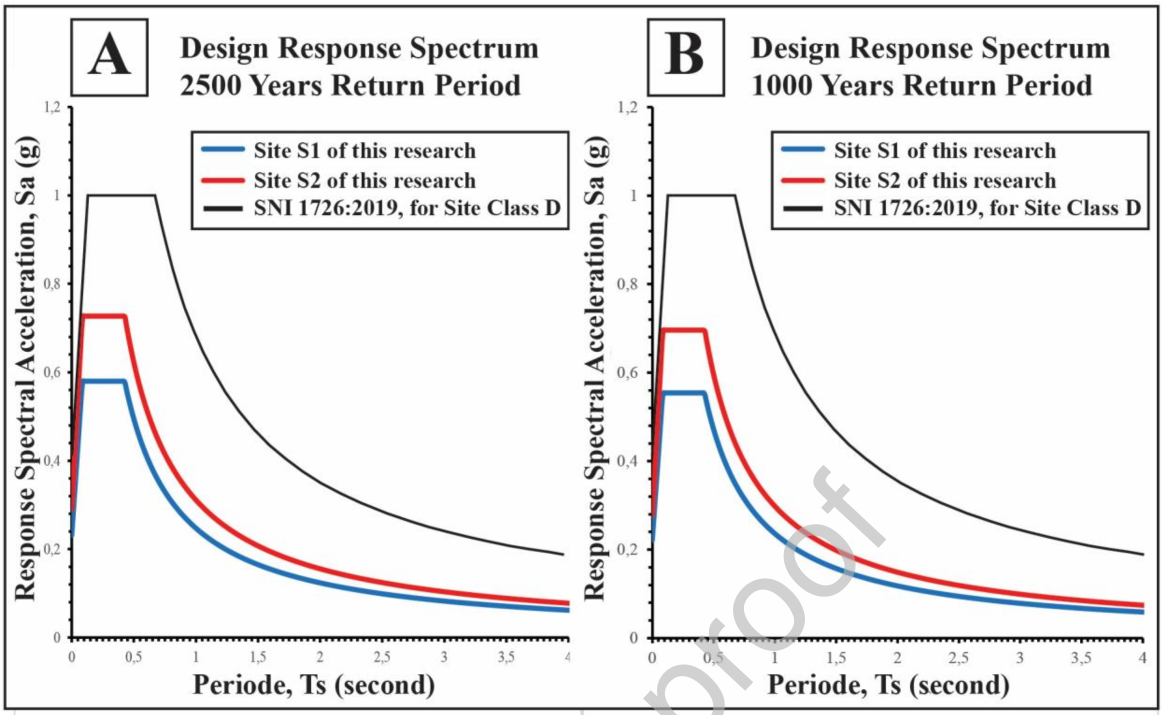

Fig. 14. (A) Design Spectral Response 2500 years. The graph shows the elastic design response spectrum for buildings and non-buildings for Location S1 and Location S2 on the SB site class, less than the national standard. (B) The graph of Spectral Response Design 1000 years shows the elastic design response spectrum for buildings and non-buildings for Locations S1 and S2 on the SB site class, which also presents a smaller value than the national standard.

Table 1. Sulawesi Empirical Magnitude Functions Adopted from (Simanjuntak, 2007; Sukamto et al.,1994; Sukamto, 2012; Simons et al., 2007; MPWH, 2017).

Line ID	Structure Segment	Type	Slipe Rate (mm/y)	Length (km)
0	Tarakan	Strike Slip	1	174
1	North Sulawesi Trench	Reverse	N/A	550
2	Gorontalo North	Strike Slip	10	76.5
3	Gorontalo South	Strike Slip	10	70
4	Tomini	Reverse	2	122
5	Tondano Fault	Normal	N/A	46
6	Palu North	Strike Slip	10	156
7	Palu South	Strike Slip	20	106
8	Palukoro North	Strike Slip	20	148
9	Palukoro South	Strike Slip	10	123
10	Makasar Strait North	Reverse	10	102
11	Saluki	Strike Slip	10	59
12	Palolo A	Normal	1	40
13	Palolo B	Normal	1	33
14	Sausu	Strike Slip	2	40
15	Tokararu	Reverse	2	53
16	Maleei	Reverse	1	50
17	Moa	Strike Slip	10	61
18	Napu	Reverse	1	30
19	Poso	Reverse	1	90
20	Kuleana	Reverse	7	39
21	Pewusai	Reverse	7	36
22	Loa	Strike Slip	7	79
23	Weluki	Reverse	7	77
24	Matano	Strike Slip	7	148
25	Batui Thrust	Reverse	1	87
26	Balantak	Strike Slip	5	178

27	Peleng	Strike Slip	1	58
28	Ambelang	Reverse	1	72
29	Lawanopo	Strike Slip	1	200
30	Tolo	Reverse	1	192
31	Buton A	Strike Slip	1	35
32	Buton B	Strike Slip	1	65
33	Makasar Strait	Reverse	5	192
34	Mamuju	Reverse	5	154
35	Walanae	Strike Slip	5	288

Table. 2. Risk Targeted MCE 2500 years Return Period

SITE	**LONG**	**LAT**	**PGA (g)**	**SS (g)**	**S1 (g)**
S1	120.6	-2.06	0.361	0.87	0.371
S2	120.97	-2.31	0.465	1.091	0.467

Table 3. Design Spectral Parameter 2500 Years Return Period

SITE	F_a	F_v	S_{MS}	S_{M1}	S_{DS}	S_{D1}
S1	1.00	1.00	0.87	0.37	0.58	0.25
S2	1.00	1.00	1.09	0.47	0.73	0.31

Table 4. Design Spectral Parameter 1000 Years Return Period

SITE	F_a	F_v	S_{MS}	S_{M1}	S_{DS}	S_{D1}
S1	1.00	1.00	0.83	0.35	0.55	0.24
S2	1.00	1.00	1.04	0.45	0.70	0.30

Declaration of Interest Statement

☒ The authors declare that they have no known competing financial interests or personal relationships that could have appeared to influence the work reported in this paper.

☐ The author is an Editorial Board Member/Editor-in-Chief/Associate Editor/Guest Editor for this journal and was not involved in the editorial review or the decision to publish this article.

☐ The authors declare the following financial interests/personal relationships which may be considered as potential competing interests: